

## Supporting Information

to

# **Pd( $\mu$ -L)<sub>4</sub>Pt vs. Pd( $\mu$ -L)<sub>4</sub>RuCl<sub>2</sub>: Chlorido co-Ligands as Defining Factors in the Host-Guest Interactions of M( $\mu$ -L)<sub>4</sub>M' Heterodimetallic Supramolecular Architectures**

Hayden B. Gearing,<sup>[a]</sup> Monika Cziferszky,<sup>[b]</sup> Tilo Söhnel,<sup>[a,c]</sup> L. James Wright,<sup>[a]</sup> James D. Crowley<sup>[c,d]</sup> and Christian G. Hartinger<sup>[a]\*</sup>

<sup>[a]</sup> School of Chemical Sciences, University of Auckland, Private Bag 92019, Auckland 1142 (New Zealand)

<sup>[b]</sup> Institute of Pharmacy/Pharmaceutical Chemistry, University of Innsbruck, Centre for Chemistry and Biomedicine, Innrain 80 - 82/IV, 6020 Innsbruck (Austria)

<sup>[c]</sup> MacDiarmid Institute for Advanced Materials and Nanotechnology, Victoria University of Wellington, PO Box 600, Wellington 6140 (New Zealand)

<sup>[d]</sup> Department of Chemistry, University of Otago, PO Box 56, Dunedin 9054 (New Zealand)

### **Contents**

Experimental procedures

Formation of cages C<sub>Pt</sub> and C<sub>Ru</sub>

Guest binding studies

Cisplatin, oxaliplatin and 5-fluorouracil as guests

X-ray crystallographic data

Host-guest MMFF models

## Experimental Procedures

### General

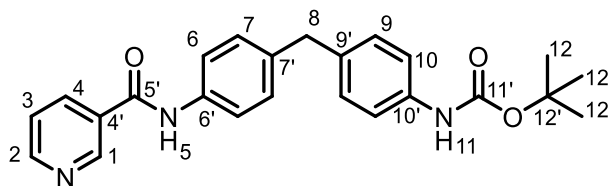
All reagents were purchased from commercial sources and used without further purification. Unless otherwise stated, reactions were conducted under an atmosphere of N<sub>2</sub>. [Pd(DMAP)<sub>4</sub>](BF<sub>4</sub>)<sub>2</sub>,<sup>[1]</sup> [Pt(3-PA)<sub>4</sub>](BF<sub>4</sub>)<sub>2</sub> (**Pt<sub>pyald</sub>**),<sup>[2]</sup> [Ru(3-PA)<sub>4</sub>Cl<sub>2</sub>] (**Ru<sub>pyald</sub>**),<sup>[3]</sup> and tert-butyl-(4-(4-aminobenzyl)phenyl)carbamate (Boc-MDA)<sup>[4]</sup> were synthesized following literature procedures. [Pd<sub>2</sub>**2**](BF<sub>4</sub>)<sub>4</sub> was formed from 5.0 mg of **2** and 5.1 mg of [Pd(CH<sub>3</sub>CN)<sub>4</sub>](BF<sub>4</sub>)<sub>2</sub> (2:1 molar ratio) in DMSO-*d*<sub>6</sub> (0.5 mL) in an NMR tube, and a <sup>1</sup>H NMR spectrum was recorded which was in line with data previously reported.<sup>[5]</sup> Solvent and reagent abbreviations include acetonitrile (CH<sub>3</sub>CN), dichloromethane (DCM), dimethylformamide (DMF), dimethyl sulfoxide (DMSO), ethyl acetate (EtOAc), diethyl ether (Et<sub>2</sub>O), and 4,4'-methylenedianiline (MDA). <sup>1</sup>H, <sup>13</sup>C{<sup>1</sup>H}, DEPTQ, COSY, NOESY, HSQC and DOSY NMR spectra were recorded in DMSO-*d*<sub>6</sub> or CD<sub>3</sub>CN on Bruker AVIII 400, 400plus or Ascend 500 NMR spectrometers at ambient temperatures. Chemical shifts (δ) are reported in parts per million (ppm). <sup>1</sup>H NMR spectra were referenced to residual solvent peaks; DMSO-*d*<sub>6</sub>, δ 2.50 ppm; CD<sub>3</sub>CN, δ 1.94 ppm. <sup>13</sup>C{<sup>1</sup>H} NMR spectra were referenced to signals associated with DMSO-*d*<sub>6</sub> (δ 39.52 ppm). <sup>1</sup>H NMR spectroscopic data are reported as chemical shift, multiplicity (s, singlet; brs, broad singlet; d, doublet; dd, doublet of doublets; ddd, doublet of doublets of doublets; dt, doublet of triplets; t, triplet; td, triplet of doublets; hept, heptet; m, multiplet), coupling constant (J) in Hertz (Hz), relative integral, and assignment. Signals in the <sup>1</sup>H and <sup>13</sup>C{<sup>1</sup>H} NMR spectra were assigned using a combination of 2D NMR experiments.

ESI-MS data were recorded on a Thermo Orbitrap Exploris 120 mass spectrometer in positive ionization mode. For MSAs **C<sup>4</sup><sub>Pt</sub>** and **C<sup>4</sup><sub>Ru</sub>**, samples were run under cold-spray conditions with the desolvation temperature set to the lowest possible setting (50 °C). Host-guest complexes were prepared in MS grade MeCN in a 1:1 or 1:5 ratio and diluted to a final concentration of 10 μM. Sample solutions were infused at 5 μL/min and ionized in the ESI source with standard conditions (3.4 kV spray voltage, ion transfer tube temperature 250 °C, vaporizer temperature 50 °C, sheath gas and auxiliary gas flow rate at 5 and 2 arbitrary units, respectively). Precursor ions were selected with an m/z window of 7 Da and were subjected to increasing amounts of normalized collision energy (NCE) in the higher-energy collisional dissociation cell. Data analysis was performed using the Xcalibur software package (Thermo Scientific). Reported m/z values refer to the most intense signal of the respective isotopic cluster.

Molecular structures were determined by single crystal X-ray diffraction measurements (XRD). XRD of single crystals of **C<sup>4</sup><sub>Pt</sub>**, **C<sup>4</sup><sub>Ru</sub>** and **C<sup>4</sup><sub>Pt</sub>CNDS** were performed on a Rigaku Oxford Diffraction XtaLAB-Synergy-S single-crystal diffractometer (Rigaku Corp., Tokyo, Japan) with

a PILATUS 200 K hybrid pixel array detector using Cu K $\alpha$  radiation ( $\lambda = 1.54184 \text{ \AA}$ ). The data were processed with the SHELXT<sup>[6]</sup> and Olex2<sup>[7]</sup> software packages (Table S2). All non-hydrogen atoms were refined anisotropically. Hydrogen atoms were inserted at calculated positions and refined with a riding model. Additional solvent molecules have been modelled by using the Squeeze procedure included in ShelXL. Solvent masks were calculated based on the solvent method included in Olex2. All compounds required modelling a partially or completely disordered structure. Mercury 2024.2.0 was used to visualize the molecular structures.<sup>[8]</sup>

tert-Butyl (4-(4-(nicotinamido)benzyl)phenyl)carbamate, **1**



Triethylamine (468  $\mu$ L, 3.68 mmol) was added to a suspension of nicotinic acid (227 mg, 1.84 mmol) and HATU (701 mg, 1.84 mmol) in acetonitrile (50 mL) and stirred at room temperature for 1.5 h. tert-butyl-(4-(4-aminobenzyl)phenyl)carbamate (500 mg, 1.68 mmol) was added and the mixture stirred at 70  $^{\circ}$ C for 16 h. The solution was cooled to room temperature and the solvent removed under reduced pressure, after which water (100 mL) was added to the residue and the mixture was sonicated for 3 h. The resulting precipitate was filtered, washed with water (2  $\times$  20 mL) and dried by suction to afford **1** as a white powder (642 mg, 95%).  $^1\text{H}$  NMR (400 MHz, DMSO- $d_6$ , 298 K)  $\delta$  10.37 (s, 1H, H-5), 9.23 (s, 1H, H-11), 9.09 (d,  $J$  = 1.7 Hz, 1H, H-1), 8.75 (dd,  $J$  = 4.8, 1.6 Hz, 1H, H-2), 8.29 – 8.25 (m, 1H, H-4), 7.67 (d,  $J$  = 8.5 Hz, 2H, H-6), 7.55 (ddd,  $J$  = 8.0, 4.9, 0.7 Hz, 1H, H-3), 7.36 (d,  $J$  = 8.4 Hz, 2H, H-7), 7.18 (d,  $J$  = 8.5 Hz, 2H, H-9), 7.10 (d,  $J$  = 8.5 Hz, 2H, H-10), 3.84 (s, 2H, H-8), 1.46 (s, 9H, H-12).  $^{13}\text{C}\{^1\text{H}\}$ -DEPTQ NMR (101 MHz, DMSO- $d_6$ , 298 K)  $\delta$  163.8 (Cq-5'), 152.8 (Cq-4'), 152.0 (C-2), 148.6 (C-1), 137.5 (Cq-10'), 137.3 (Cq-6'), 136.7 (Cq-9'), 135.4 (C-4), 134.9 (Cq-7'), 130.6 (Cq-11'), 128.8 (C-9 & 10), 123.5 (C-3), 120.5 (C-6), 118.3 (C-7), 78.8 (Cq-12'), 40.1 (C-8), 28.1 (C-12). HR-ESI-MS:  $m/z$  404.1967 ( $[\text{M} + \text{H}]^+$   $m/z_{\text{calc}}$  404.1969), 807.3859 ( $[\text{2M} + \text{H}]^+$   $m/z_{\text{calc}}$  807.3865).

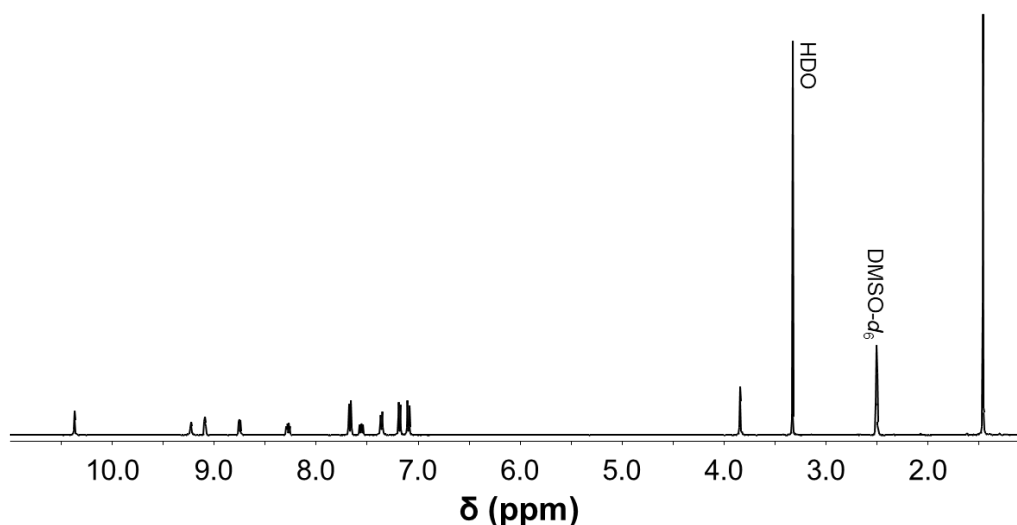


**Figure S1.**  $^1\text{H}$  NMR spectrum (400MHz, DMSO- $d_6$ , 298 K) of **1**.

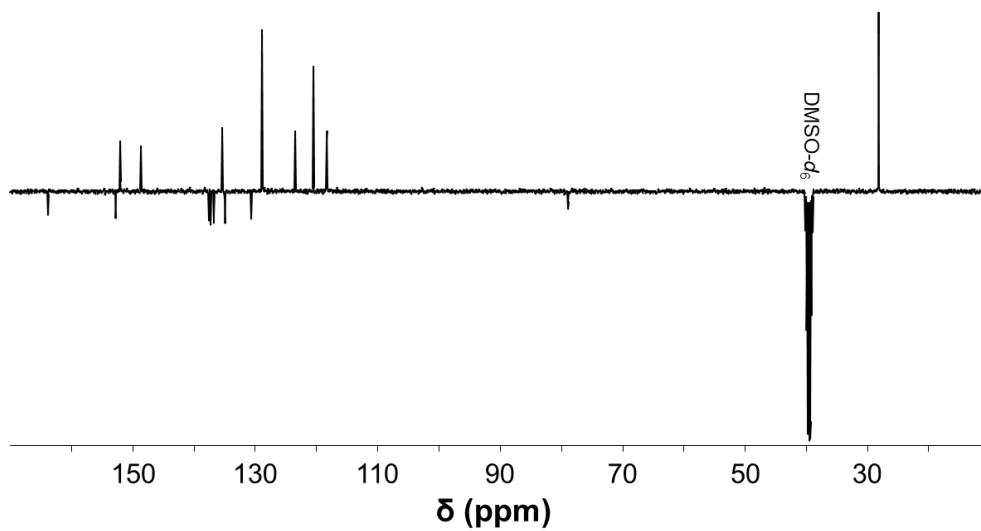


**Figure S2.**  $^{13}\text{C}\{^1\text{H}\}$ -DEPT-Q NMR spectrum (400MHz, DMSO- $d_6$ , 298 K) of **1**.

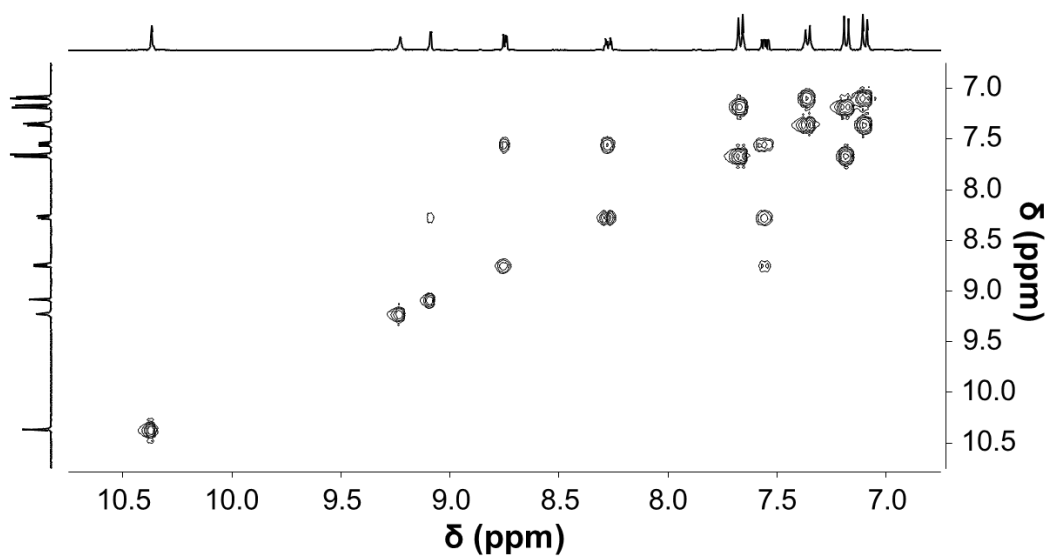


**Figure S3.** COSY NMR spectrum (400MHz, DMSO- $d_6$ , 298 K) of **1**.

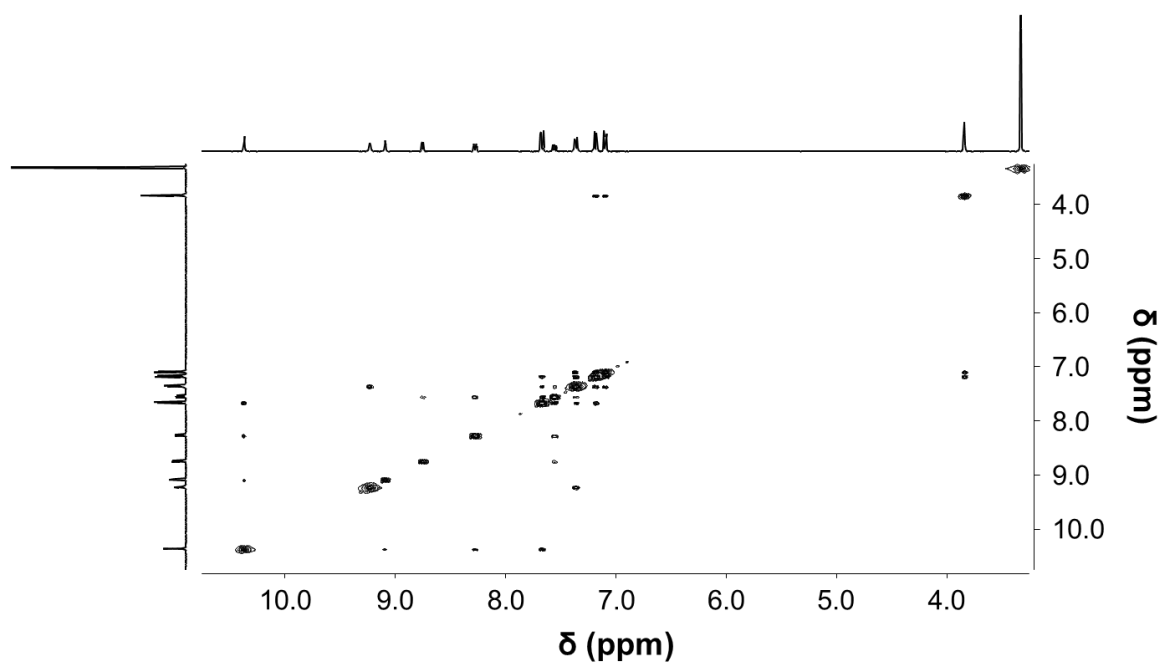


Figure S4. NOESY NMR spectrum (400MHz, DMSO- $d_6$ , 298 K) of 1.

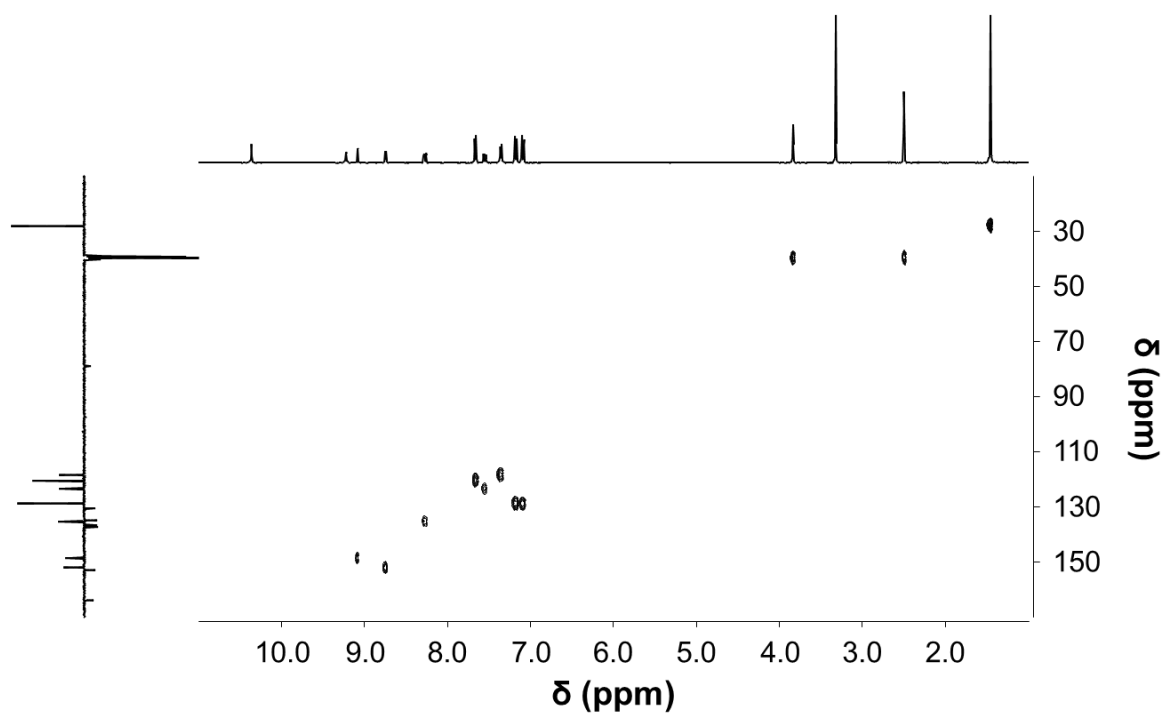
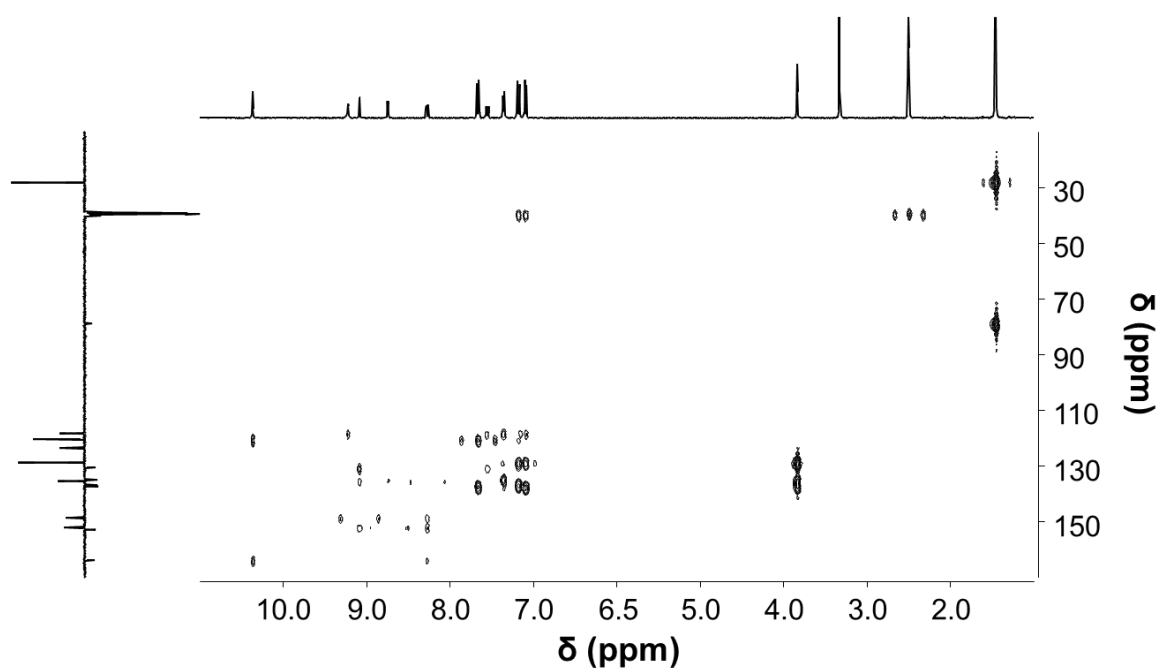
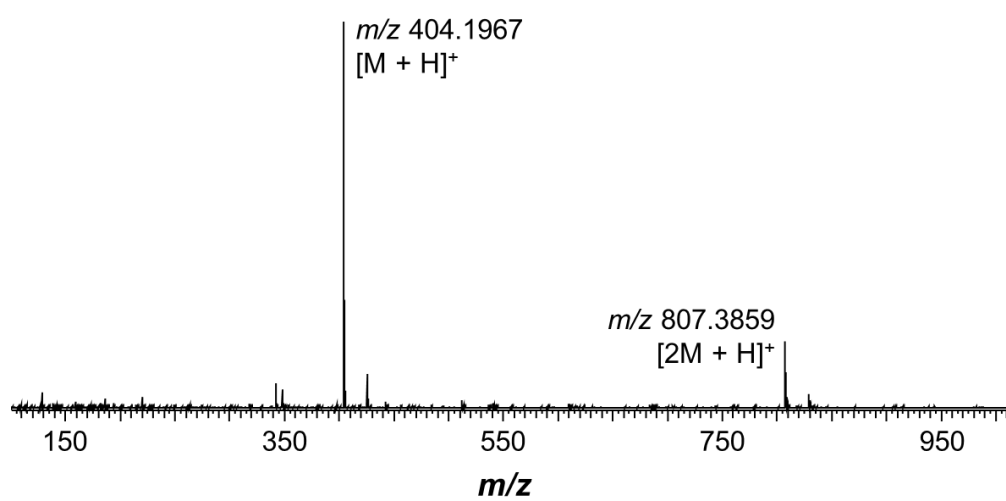


Figure S5. HSQC NMR spectrum (400MHz, DMSO- $d_6$ , 298 K) of 1.

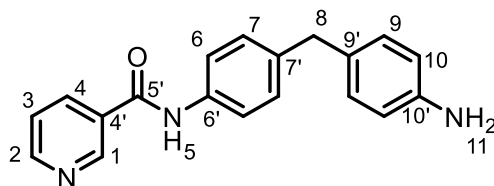


**Figure S6.** HMBC NMR spectrum (400MHz, DMSO- $d_6$ , 298 K) of **1**.



**Figure S7.** HR-ESI-mass spectrum ( $\text{CH}_3\text{CN}$ ) of **1**.

*N*-(4-(4-Aminobenzyl)phenyl)nicotinamide, compound **2**.



Trifluoroacetic acid (2 mL) was added dropwise to a suspension of **1** (543 mg, 1.35 mmol) in chloroform (10 mL) and the mixture was stirred for 3 h. The volatiles were removed *in vacuo* and saturated aqueous sodium bicarbonate (50 mL) was added and the solution stirred until the bubbling of CO<sub>2</sub> stopped. The mixture was filtered, washed with water (2 × 20 mL) and dried by suction to give **2** as a white solid (376 mg, 92%). <sup>1</sup>H NMR (400 MHz, DMSO-*d*<sub>6</sub>, 298 K) δ 10.35 (s, 1H, H-5), 9.09 (dd, *J* = 2.2, 0.7 Hz, 1H, H-1), 8.75 (dd, *J* = 4.8, 1.6 Hz, 1H, H-2), 8.27 (ddd, *J* = 8.0, 2.2, 1.8 Hz, 1H, H-4), 7.65 (d, *J* = 8.5 Hz, 2H, H-6), 7.55 (ddd, *J* = 8.0, 4.8, 0.8 Hz, 1H, H-3), 7.16 (d, *J* = 8.5 Hz, 2H, H-7), 6.86 (d, *J* = 8.4 Hz, 2H, H-9), 6.49 (d, *J* = 8.4 Hz, 2H, H-10), 4.87 (brs, 2H, H-11), 3.73 (s, 2H, H-8). <sup>13</sup>C{<sup>1</sup>H}-DEPTQ NMR (101 MHz, DMSO) δ 163.8 (Cq-5'), 152.0 (C-2), 148.6 (C-1), 146.6 (Cq-10'), 138.1 (Cq-6'), 136.5 (Cq-7'), 135.4 (C-4), 130.6 (Cq-4'), 129.1 (C-9), 128.7 (C-7), 128.4 (Cq-9'), 123.5 (C-3), 120.4 (C-6), 114.0 (C-10), 39.9 (C-8). ESI-MS: *m/z* 304.1442 ([*M* + *H*]<sup>+</sup> *m/z*<sub>calc</sub> 304.1445). HR-ESI-MS: *m/z* 304.1442 ([*M* + *H*]<sup>+</sup> *m/z*<sub>calc</sub> 304.1445).

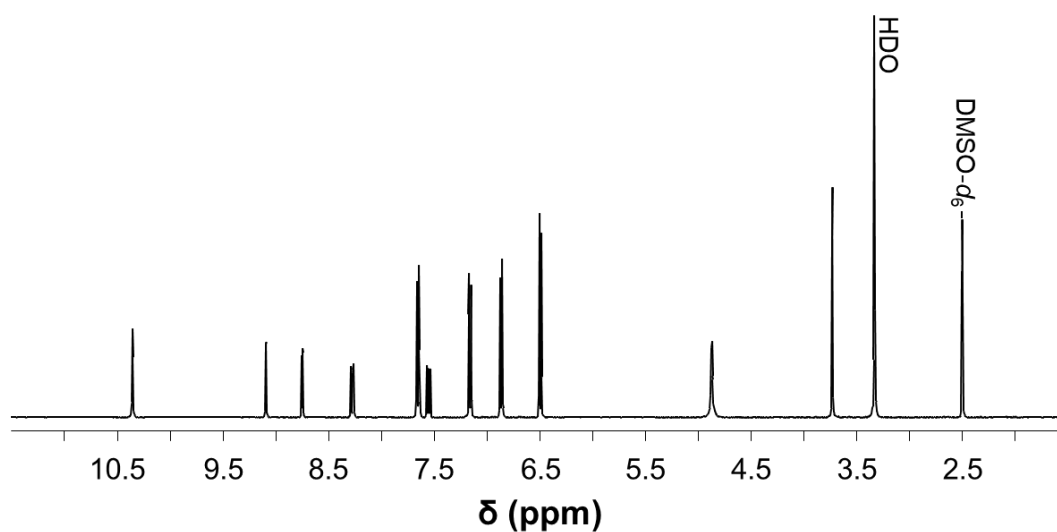


**Figure S8.** <sup>1</sup>H NMR spectrum (400MHz, DMSO-*d*<sub>6</sub>, 298 K) of **2**.

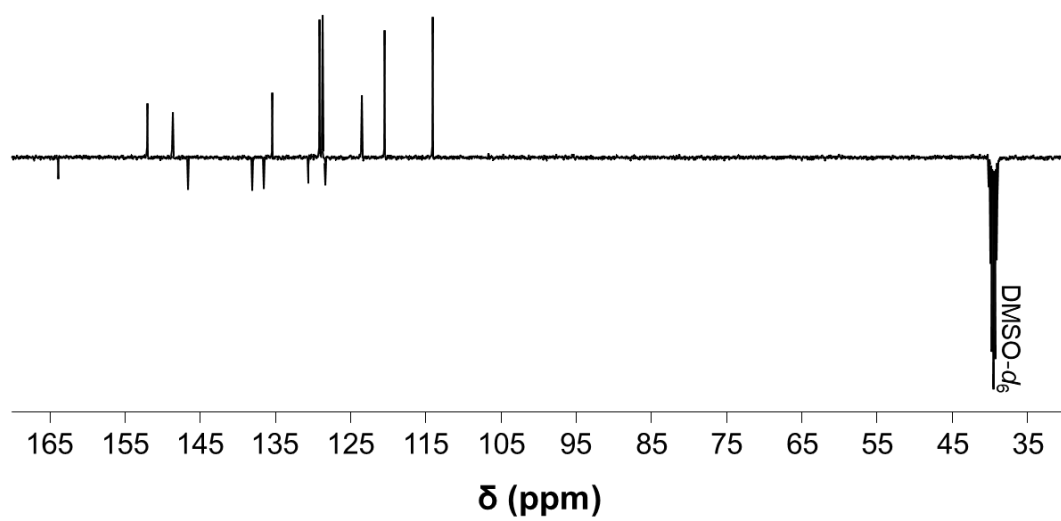


**Figure S9.**  $^{13}\text{C}\{^1\text{H}\}$ -DEPT-Q NMR spectrum (400MHz, DMSO- $d_6$ , 298 K) of **2**.

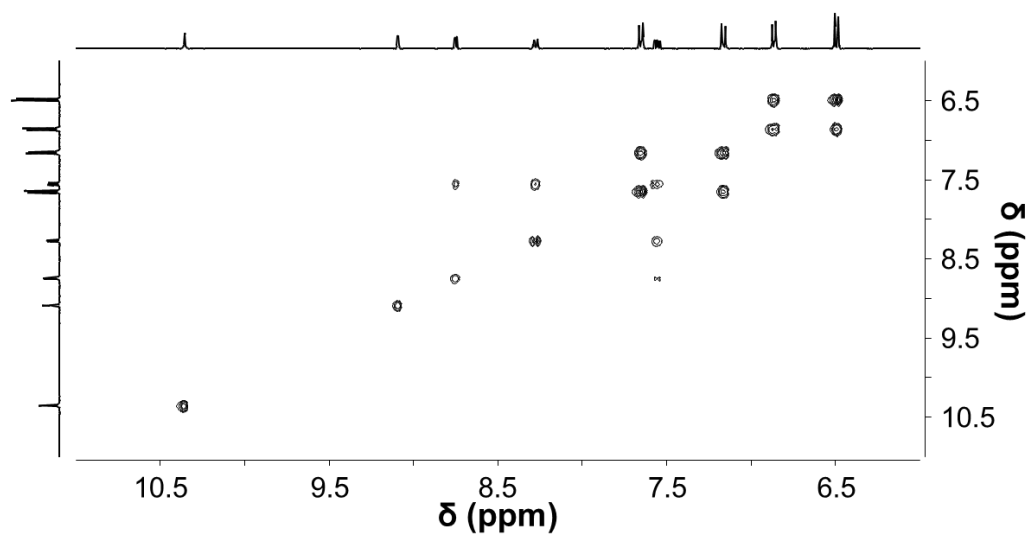


**Figure S10.** COSY NMR spectrum (400MHz, DMSO- $d_6$ , 298 K) of **2**.

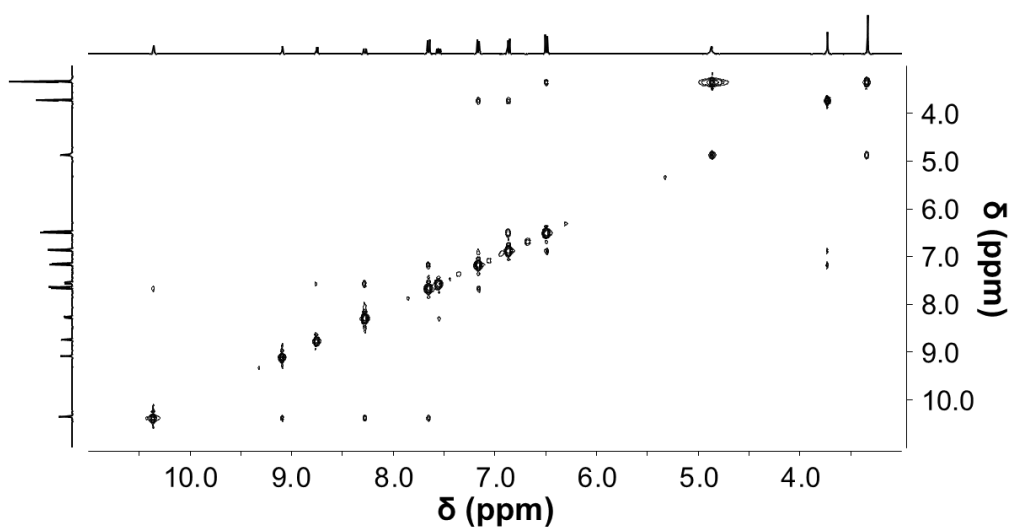


**Figure S11.** NOESY NMR spectrum (400MHz, DMSO- $d_6$ , 298 K) of **2**.

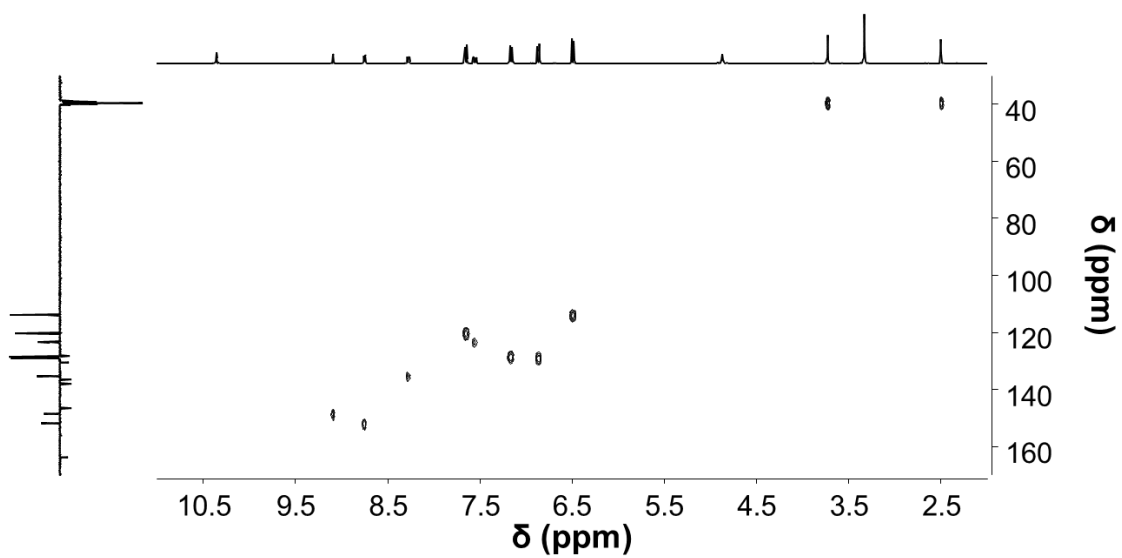


**Figure S12.** HSQC NMR spectrum (400MHz, DMSO- $d_6$ , 298 K) of **2**.

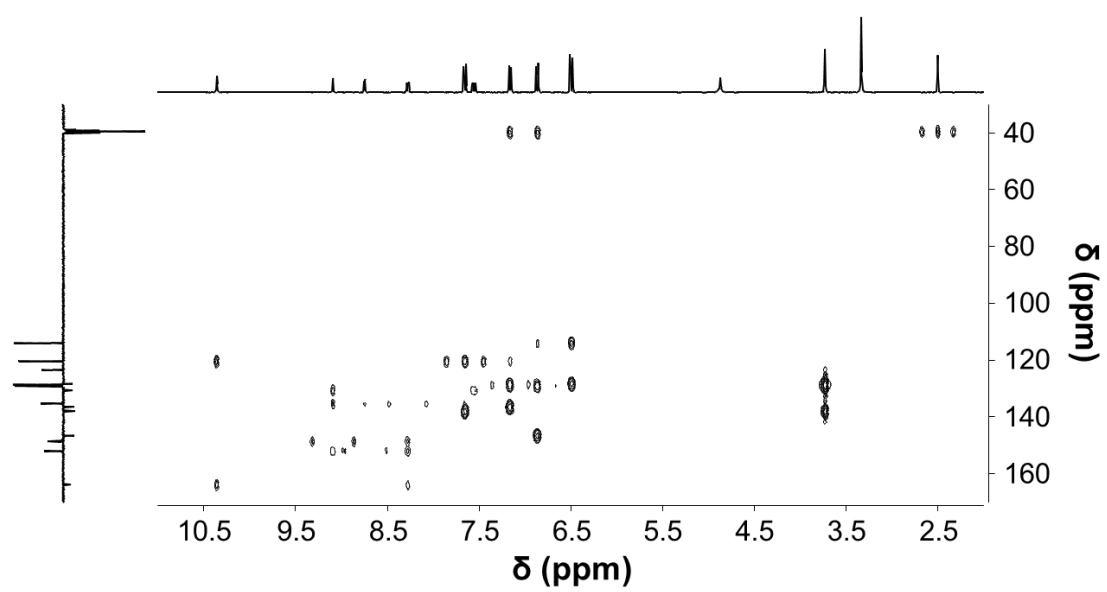


**Figure S13.** HMBC NMR spectrum (400MHz, DMSO- $d_6$ , 298 K) of **2**.

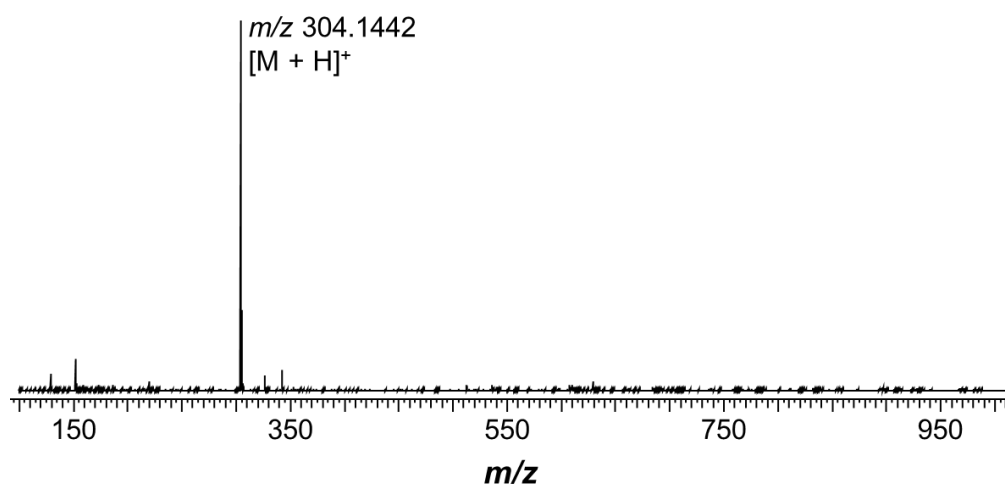
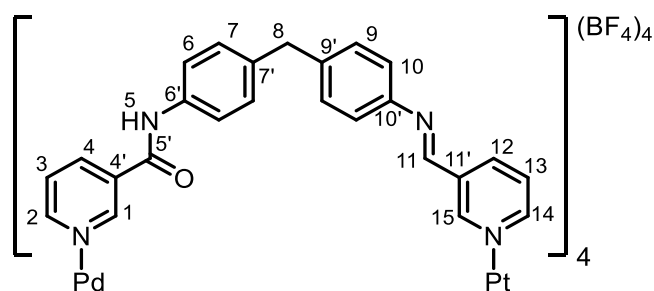


**Figure S14.** HR-ESI-mass spectrum ( $\text{CH}_3\text{CN}$ ) of **2**.

## Synthesis of **C**<sup>4</sup><sub>Pt</sub>



**2** (80.0 mg, 0.264 mmol), [Pd(CH<sub>3</sub>CN)<sub>4</sub>](BF<sub>4</sub>)<sub>2</sub> (29.3 mg, 65.9 μmol), and **Pt**<sub>pyald</sub> (52.6 mg, 65.9 μmol) were combined in dry DMSO (3 mL) and stirred for 24 h. EtOAc (40 mL) was added to the solution and the precipitate was filtered, washed with EtOAc (3 × 10 mL), Et<sub>2</sub>O (10 mL), and DCM (2 × 10 mL) and dried by suction to afford **C** as an off-white powder (134 mg, 92 %). <sup>1</sup>H NMR (400 MHz, DMSO-*d*<sub>6</sub>) δ 10.58 (s, 4H, H-5), 9.94 (d, *J* = 1.8 Hz, 4H, H-1), 9.85 (d, *J* = 1.3 Hz, 4H, H-15), 9.44 (dd, *J* = 5.8, 0.9 Hz, 4H, H-2), 9.36 (dd, *J* = 5.9, 1.0 Hz, 4H, H-14), 8.60 (s, 4H, H-11), 8.52 – 8.48 (m, 4H, H-4), 8.46 – 8.43 (m, 4H, H-12), 7.89 (td, *J* = 7.8, 6.1 Hz, 8H, H-3 & 13), 7.53 (d, *J* = 8.5 Hz, 8H, H-6), 7.34 – 7.17 (m, 24H, H-7, 9 & 10), 3.99 (s, 8H, H-8). <sup>13</sup>C NMR (101 MHz, DMSO-*d*<sub>6</sub>) δ 162.0 (Cq-5'), 156.3 (C-11), 153.1 (C-2), 153.0 (C-14), 151.1 (C-1), 150.8 (C-15), 148.4 (Cq-10'), 140.9 (C-12), 140.5 (Cq-9'), 139.2 (C-4), 137.3 (Cq-7'), 136.0 (Cq-6'), 135.0 (Cq-11'), 134.0 (Cq-4'), 129.5 (C-7 & 9), 129.4 (C-7 & 9), 127.8 (C-13), 127.0 (C-3), 121.6 (C-6), 121.2 (C-10), C-8 resonance under DMSO-*d*<sub>6</sub> residual peak (Figure S18). HR-ESI-MS: *m/z* 467.6310 ([M – 4BF<sub>4</sub>]<sup>14+</sup> *m/z*<sub>calc</sub> 467.6311).

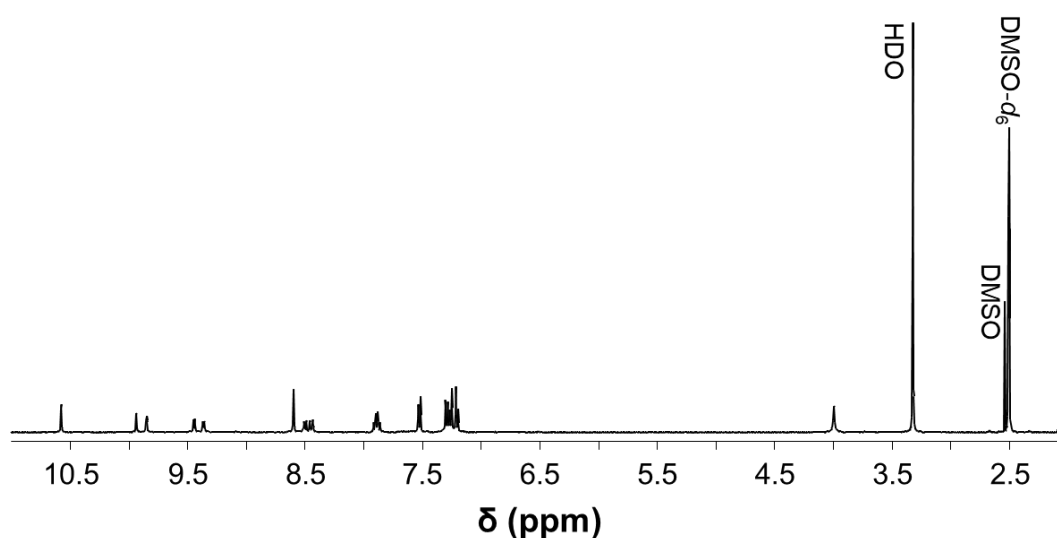


**Figure S15.** <sup>1</sup>H NMR spectrum (400MHz, DMSO-*d*<sub>6</sub>, 298 K) of **C**<sup>4</sup><sub>Pt</sub>.

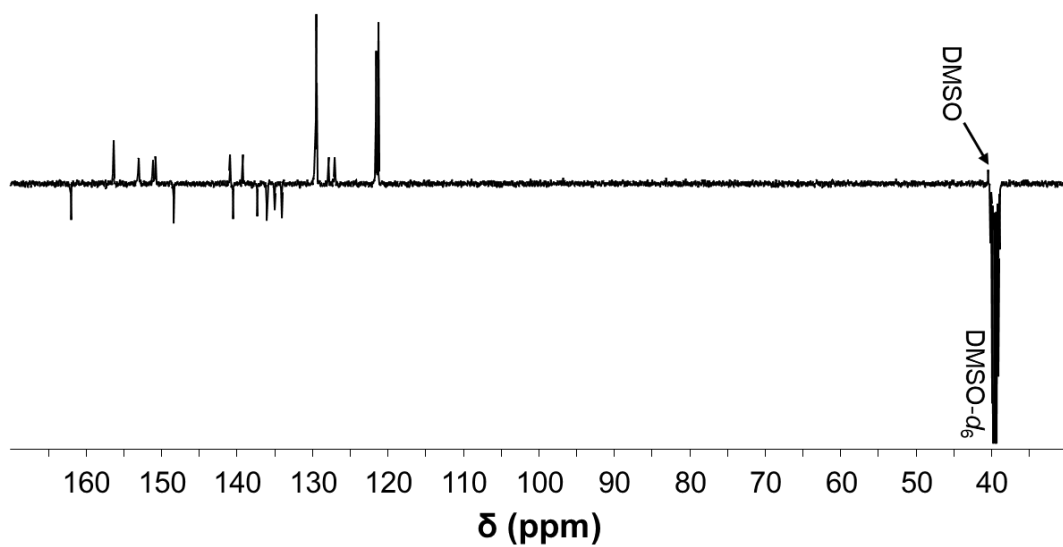


**Figure S16.**  $^{13}\text{C}\{^1\text{H}\}$ -DEPT-Q NMR spectrum (400MHz, DMSO- $d_6$ , 298 K) of  $\text{C}^4_{\text{Pt}}$ .

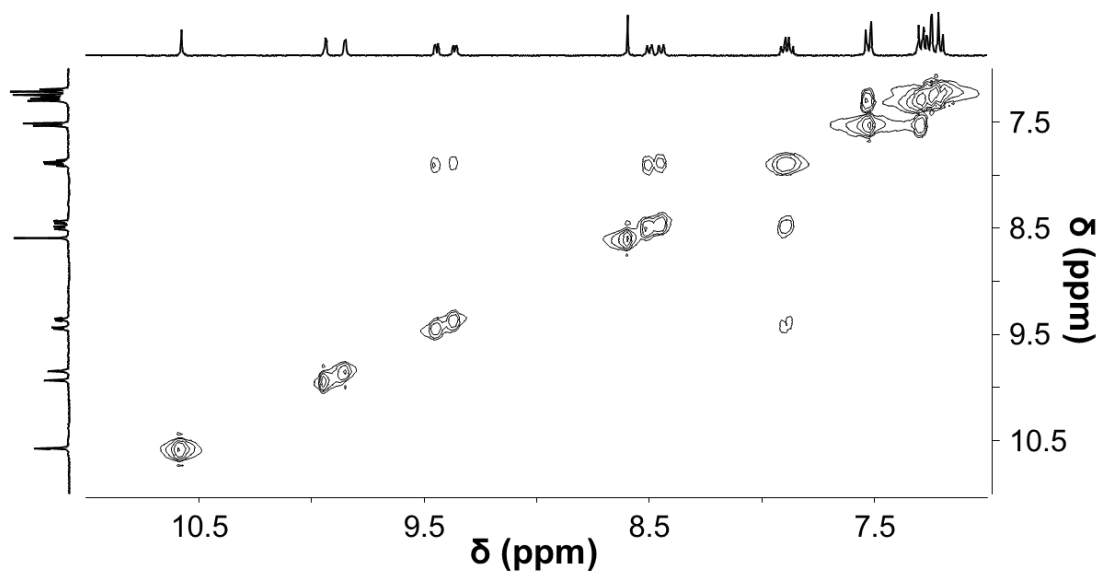


**Figure S17.** COSY NMR spectrum (400MHz, DMSO- $d_6$ , 298 K) of  $\text{C}^4_{\text{Pt}}$ .

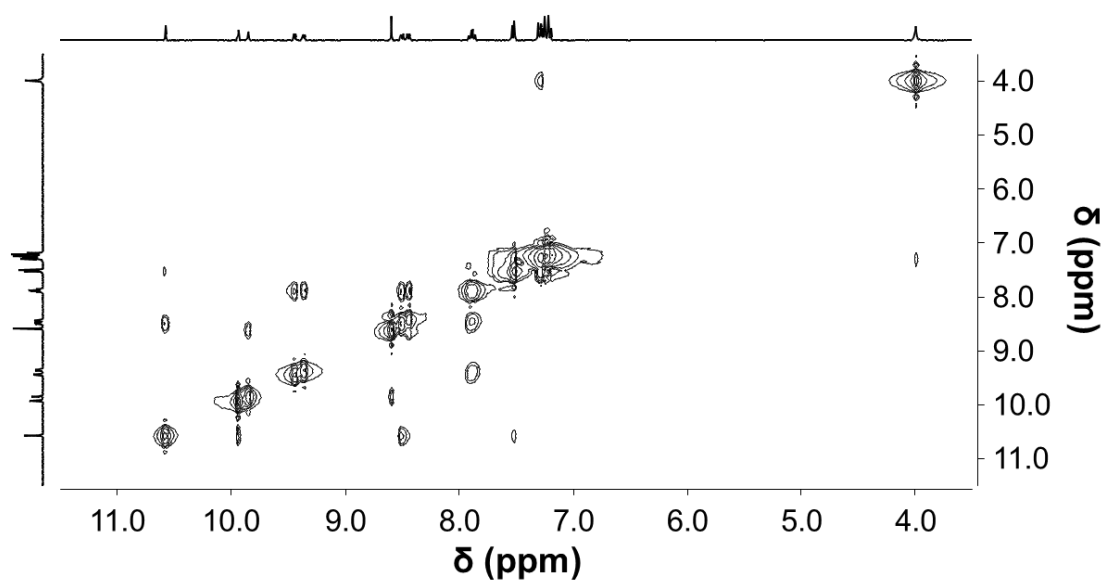


**Figure S18.** NOESY NMR spectrum (400MHz, DMSO- $d_6$ , 298 K) of  $C^4Pt$ .

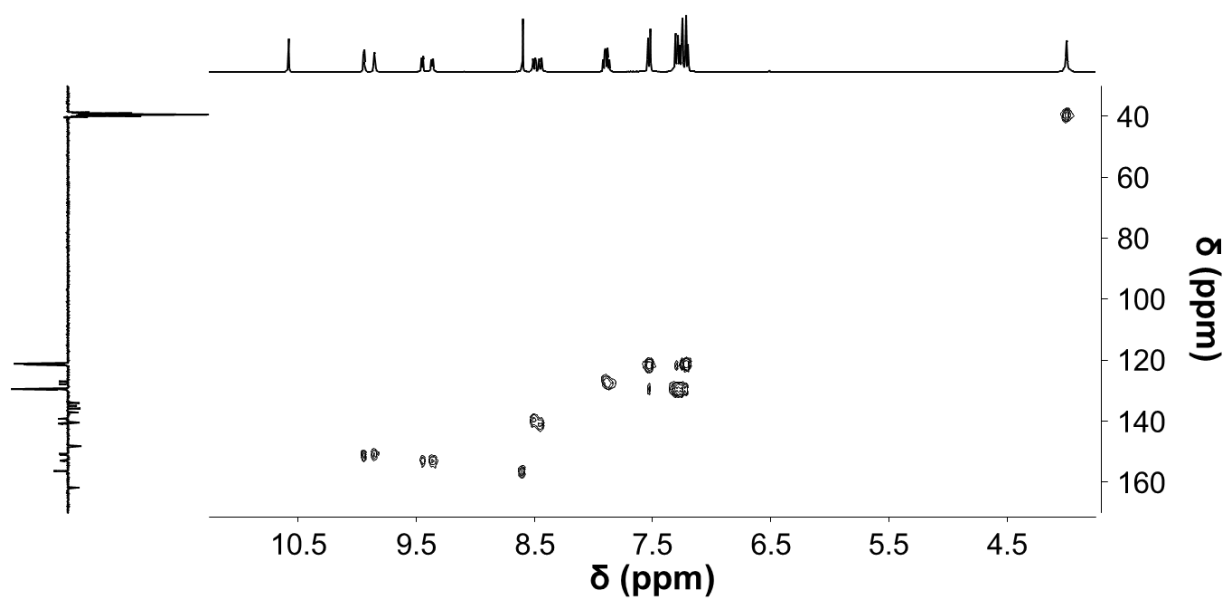


**Figure S19.** HSQC NMR spectrum (400MHz, DMSO- $d_6$ , 298 K) of  $C^4Pt$ .

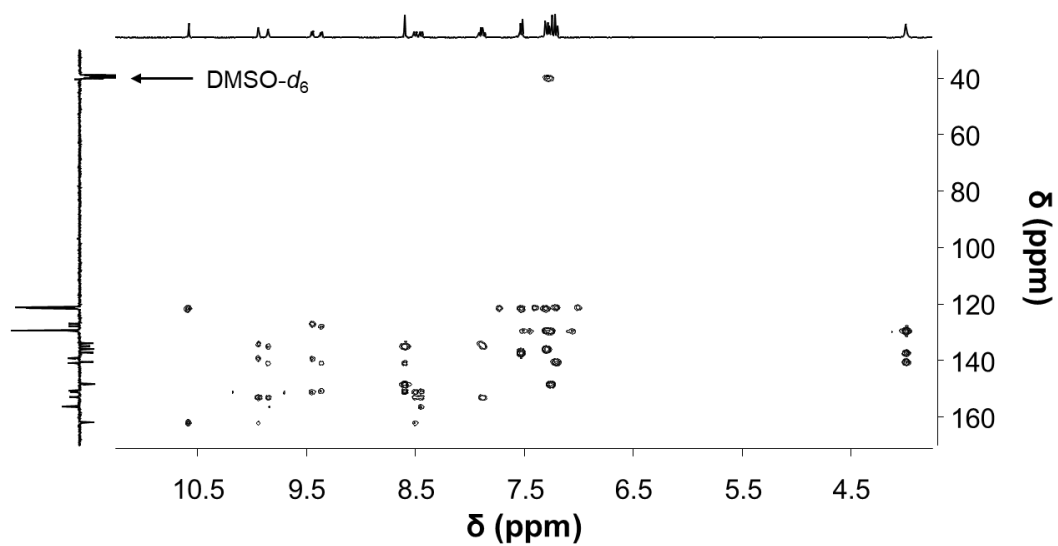


**Figure S20.** HMBC NMR spectrum (400MHz, DMSO- $d_6$ , 298 K) of  $C^4_{Pt}$ .

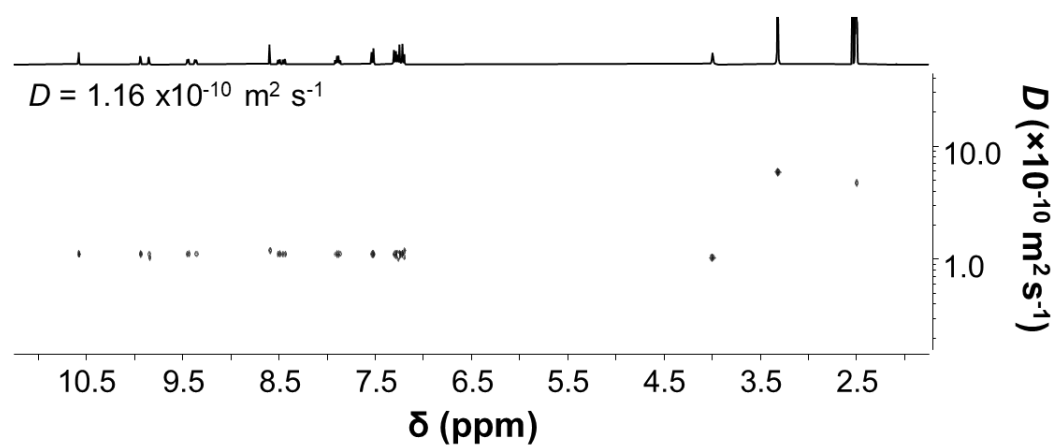


**Figure S21.** DOSY NMR spectrum (400MHz, DMSO- $d_6$ , 298 K) of  $C^4_{Pt}$ .

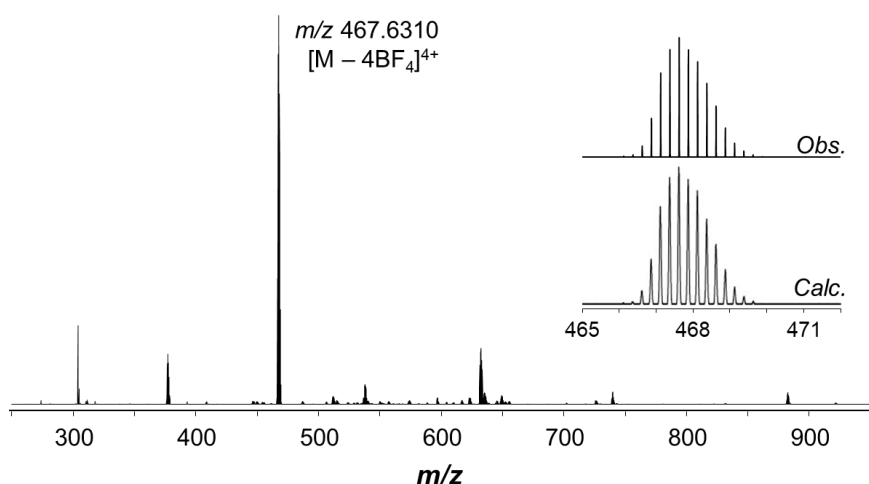
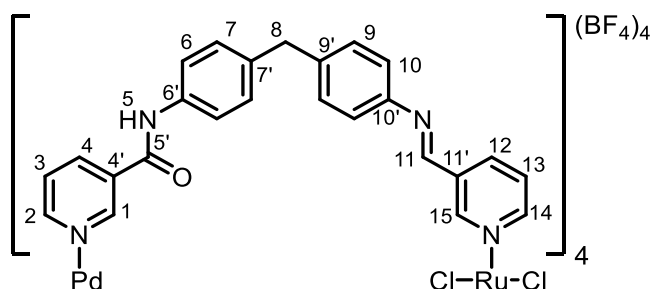


**Figure S22.** HR-ESI-mass spectrum (DMSO/CH<sub>3</sub>CN) of **C<sup>4</sup><sub>Pt</sub>**. The inset is the observed isotopic pattern (top) of [M – 4BF<sub>4</sub>]<sup>4+</sup> compared to the simulated isotopic pattern of the same ion (bottom).

#### Preparation of **C<sup>4</sup><sub>Ru</sub>**



**2** (11.2 mg, 36.9  $\mu\text{mol}$ ), [Pd(CH<sub>3</sub>CN)<sub>4</sub>](BF<sub>4</sub>)<sub>2</sub> (5.37 mg, 12.09  $\mu\text{mol}$ ), and **Ru<sub>pyald</sub>** (5.34 mg, 8.89  $\mu\text{mol}$ ) were dissolved in 1120, 734, and 1078  $\mu\text{L}$  of DMSO-*d*<sub>6</sub>, respectively. 1.0 mL of the solutions of **2** and **Ru<sub>pyald</sub>**, and 0.5 mL of the [Pd(CH<sub>3</sub>CN)<sub>4</sub>](BF<sub>4</sub>)<sub>2</sub> solution were combined and mixed for 24 h (Figure S30) which demonstrated quantitative conversion. The experiment was repeated in DMSO but **C<sup>4</sup><sub>Ru</sub>** was found to degrade during workup. Therefore, all further studies were done with stock solutions of **C<sup>4</sup><sub>Ru</sub>** (3.3 mM) in DMSO (analyzed by NMR after spiking with DMSO-*d*<sub>6</sub> to confirm absence of impurities) or DMSO-*d*<sub>6</sub>. <sup>1</sup>H NMR (400 MHz, DMSO-*d*<sub>6</sub>, 298 K)  $\delta$  10.48 (s, 4H, H-5), 9.88 (d, *J* = 1.7 Hz, 4H, H-1), 9.40 (d, *J* = 5.4 Hz, 4H, H-2), 9.01 (s, 4H, H-15), 8.80 (d, *J* = 4.3 Hz, 4H, H-14), 8.53 – 8.45 (m, 8H, H-4 & 11), 8.28 (d, *J* = 8.0 Hz, 4H, H-12), 7.84 (dd, *J* = 7.9, 5.8 Hz, 4H, H-3), 7.52 – 7.42 (m, 12H, H-6 & 13), 7.20 (d, *J* = 8.4 Hz, 8H, H-9), 7.11 (dd, *J* = 8.4, 1.8 Hz, 16H, H-7 & 10), 3.91 (s, 8H, H-8). <sup>13</sup>C{<sup>1</sup>H}-DEPT-Q NMR (101 MHz, DMSO-*d*<sub>6</sub>, 298 K)  $\delta$  161.4 (Cq-5'), 159.0 (C-14), 157.7 (C-15), 157.5 (C-11), 152.8

(C-2), 151.5 (C-1), 148.9 (Cq-10'), 139.7 (Cq-9'), 138.7 (C-4), 138.0 (Cq-6'), 135.7 (Cq-7'), 134.0 (C-12), 133.5 (Cq-4'), 131.3 (Cq-11'), 129.6 (C-9), 128.8 (C-7), 126.7 (C-3), 123.7 (C-13), 121.4 (C-6), 121.2 (C-10), C-8 resonance under DMSO- $d_6$  residual peak (Figure S25).  
HR-ESI-MS:  $m/z$  924.2009 ( $[M - 2BF_4]^{2+}$   $m/z_{calc}$  924.2011).

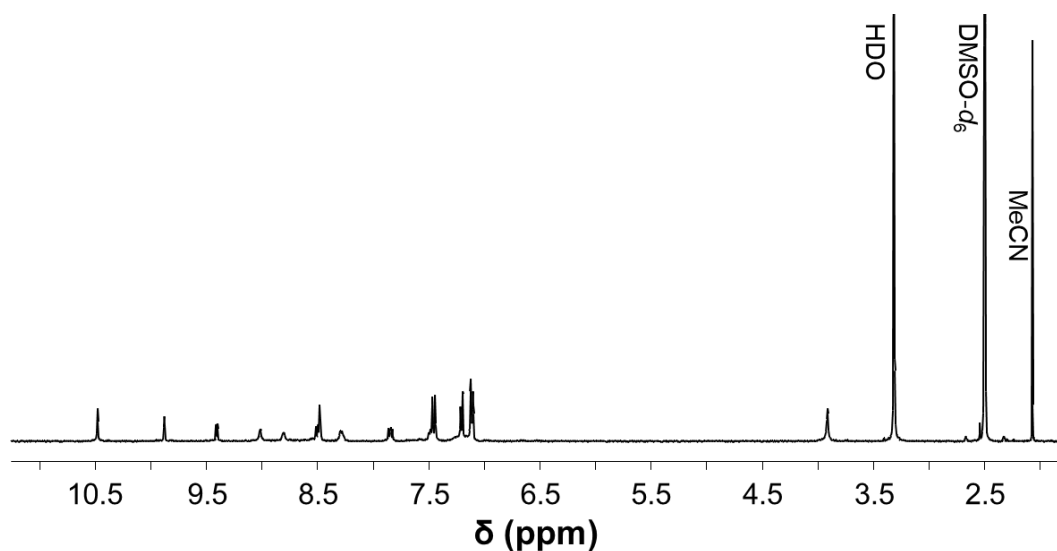


**Figure S23.**  $^1H$  NMR spectrum (400MHz, DMSO- $d_6$ , 298 K) of  $C^4_{Ru}$ .

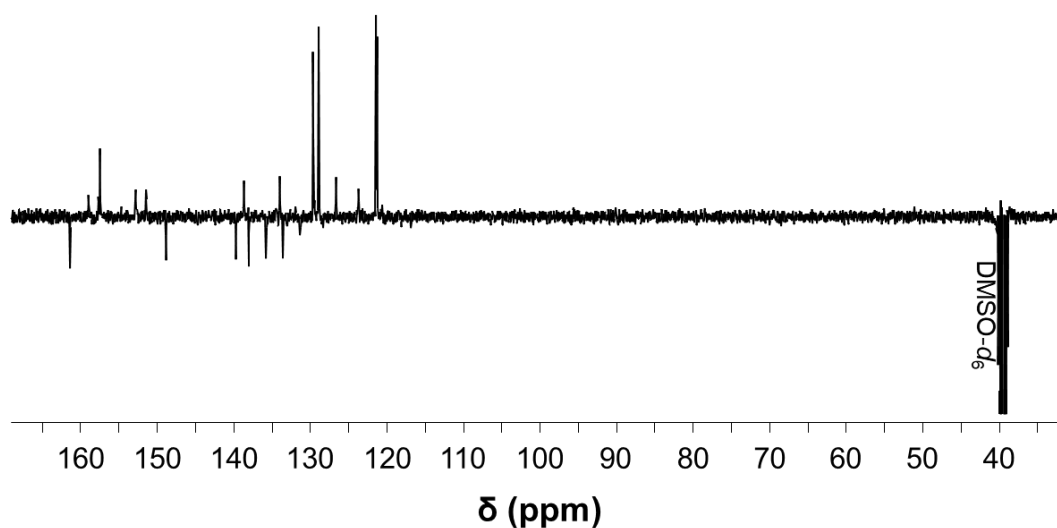


**Figure S24.**  $^{13}C\{^1H\}$ -DEPT-Q NMR spectrum (400MHz, DMSO- $d_6$ , 298 K) of  $C^4_{Ru}$ .

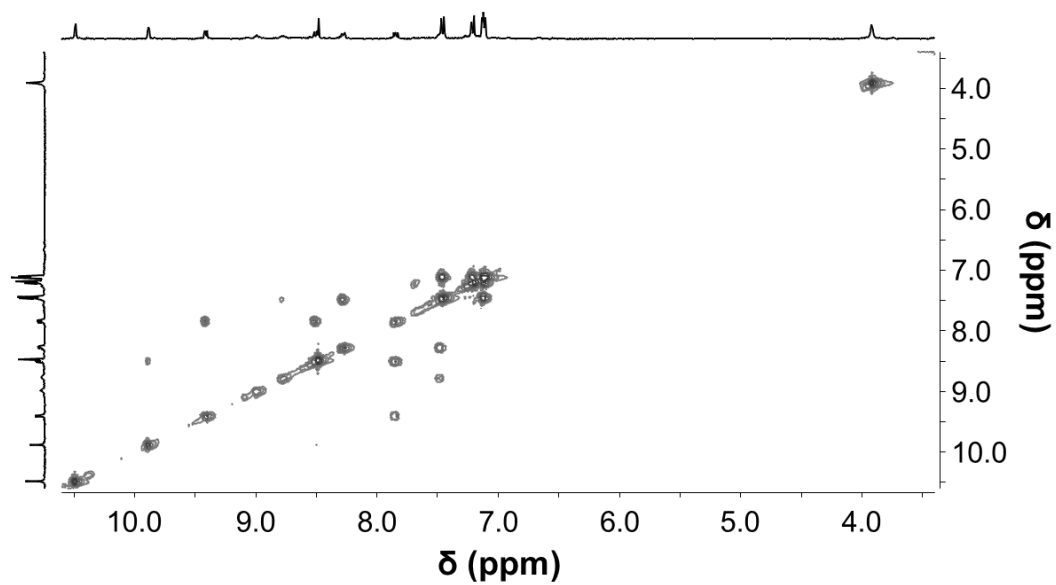


Figure S25. COSY NMR spectrum (400MHz, DMSO-*d*<sub>6</sub>, 298 K) of C<sup>4</sup>Ru.

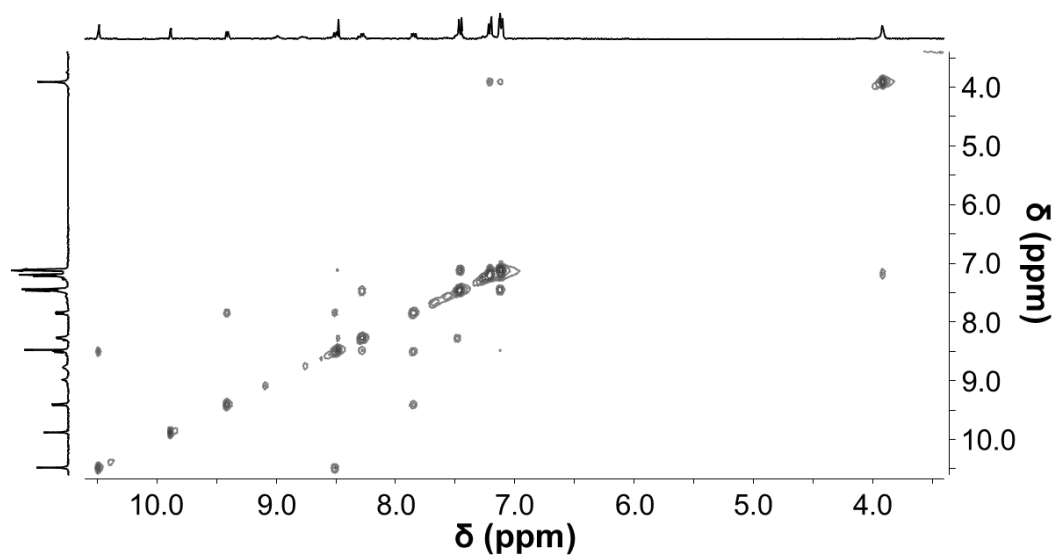


Figure S26. NOESY NMR spectrum (400MHz, DMSO-*d*<sub>6</sub>, 298 K) of C<sup>4</sup>Ru.

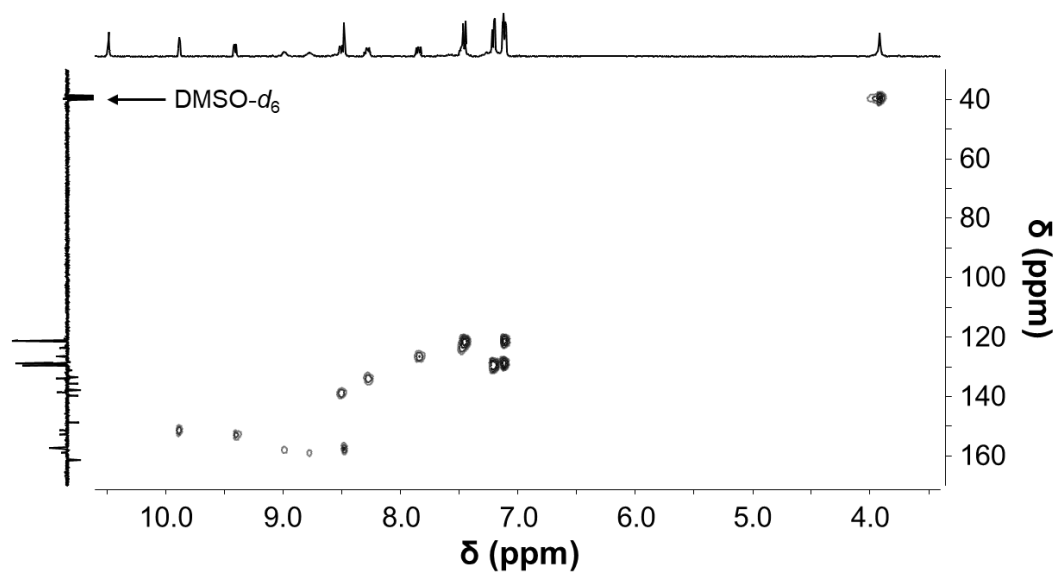


Figure S27. HSQC NMR spectrum (400MHz, DMSO- $d_6$ , 298 K) of  $C^4Ru$ .

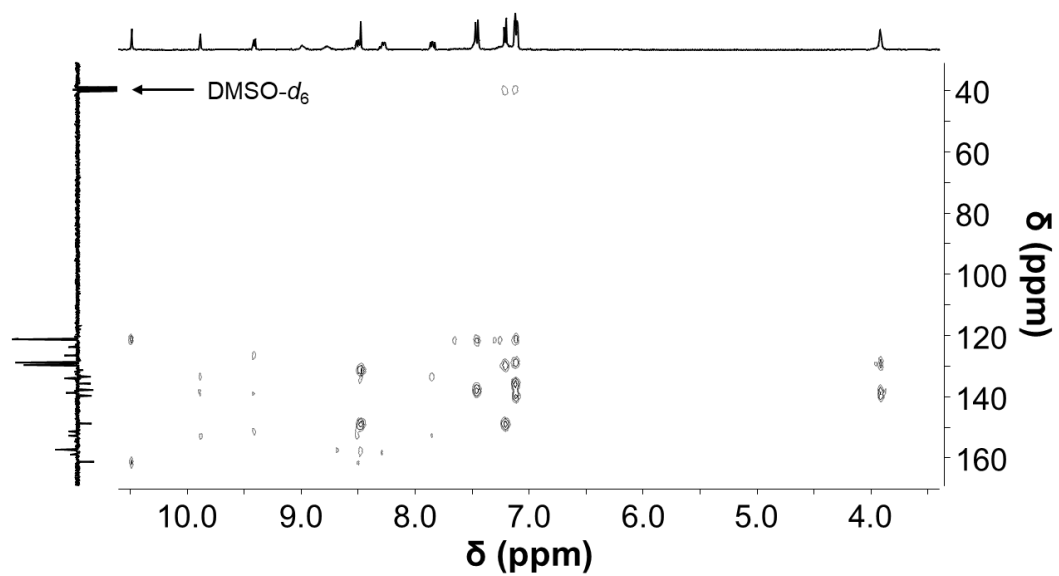
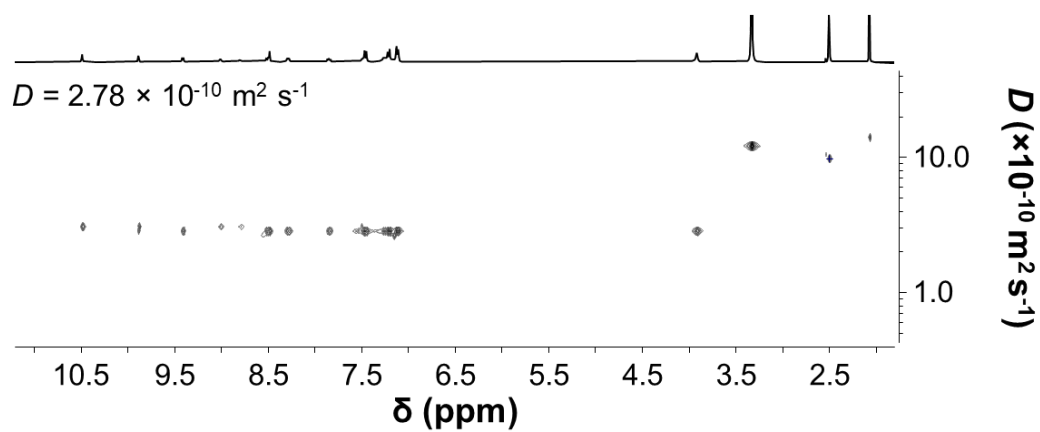
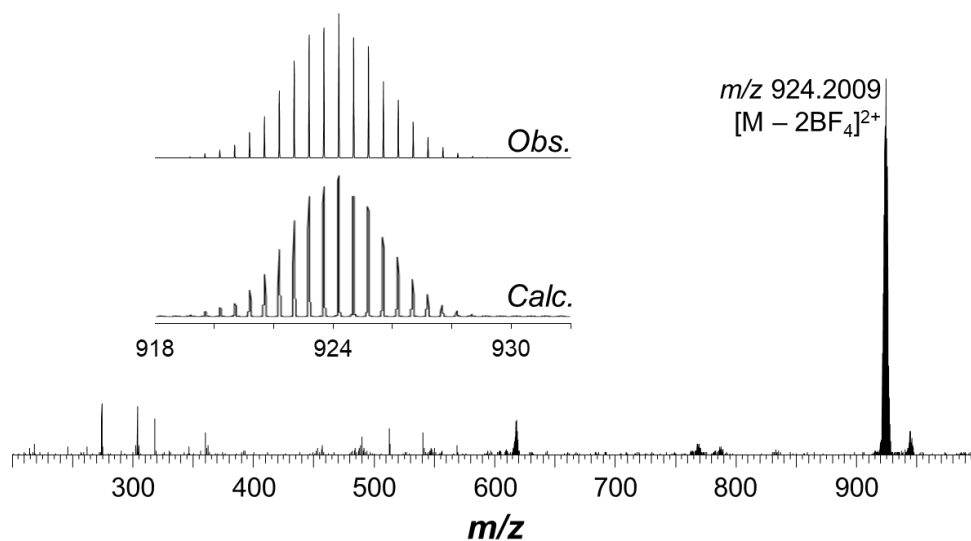


Figure S28. HMBC NMR spectrum (400MHz, DMSO- $d_6$ , 298 K) of  $C^4Ru$ .



**Figure S29.** DOSY NMR spectrum (400MHz, DMSO- $d_6$ , 298 K) of  $\text{C}^4_{\text{Ru}}$ .



**Figure S30.** HR-ESI-mass spectrum (DMSO/ $\text{CH}_3\text{CN}$ ) of  $\text{C}^4_{\text{Ru}}$ . The inset is the observed isotopic pattern (top) of  $[\text{M} - 2\text{BF}_4]^{4+}$  compared to the simulated isotopic pattern of the same ion (bottom).

## Formation of cages $C^4_{Pt}$ and $C^4_{Ru}$

Initial assessment of the assembly of  $C^4_{Pt}$  and  $C^4_{Ru}$  was carried out at small scale in an NMR tube.  $^1H$  NMR spectra were recorded 30 min, 24 h, and 48 h after addition of reagents. Complete conversion of the starting materials to the respective cage was observed after 24 h, with no noticeable change in the  $^1H$  NMR spectra between 24 and 48 h. For comparison, the spectrum of  $[Pd_2\mathbf{2}_4](BF_4)_4$  is included in Figure S31, as this is a kinetic product in the formation of each cage.<sup>[5]</sup>

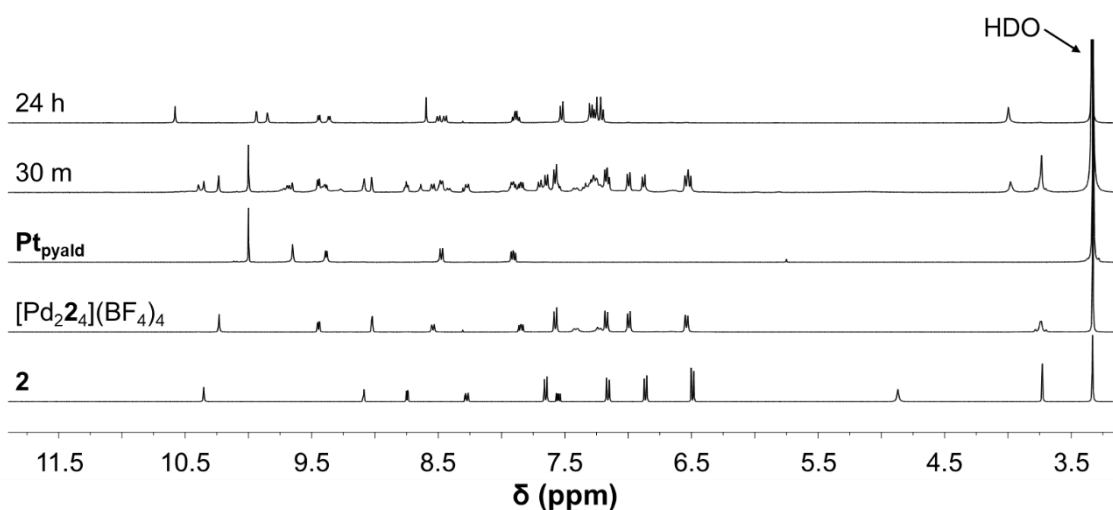


**Figure S31.** Stacked  $^1H$  NMR spectra (400 MHz, DMSO- $d_6$ , 298 K) of the formation of  $C^4_{Pt}$  from **2**,  $[Pd(CH_3CN)_4](BF_4)_2$ , and  $Pt_{pyald}$  after 30 m and 24 h.

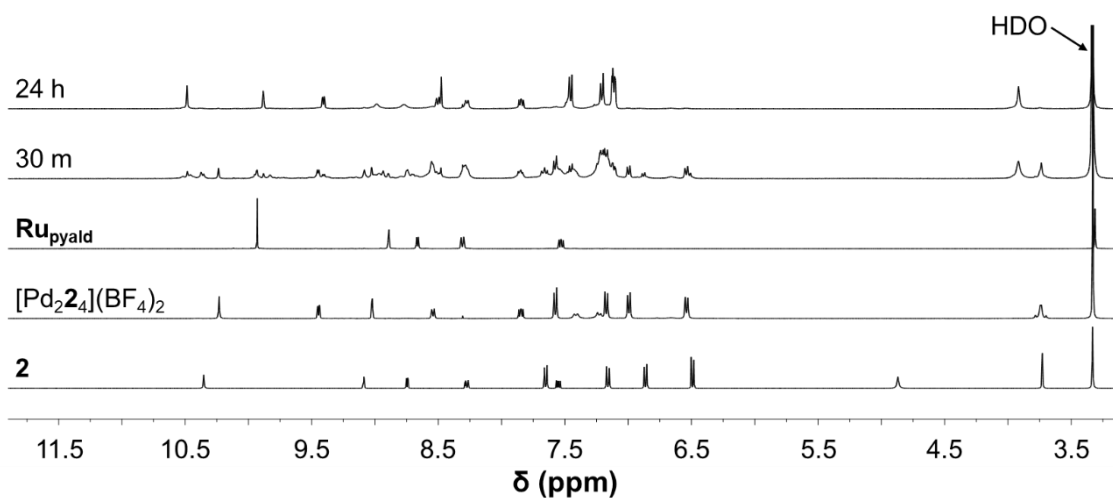


**Figure S32.** Stacked  $^1H$  NMR spectra (400 MHz, DMSO- $d_6$ , 298 K) of the formation of  $C^4_{Ru}$  from **2**,  $[Pd(CH_3CN)_4](BF_4)_2$ , and  $Ru_{pyald}$  after 30 m and 24 h.

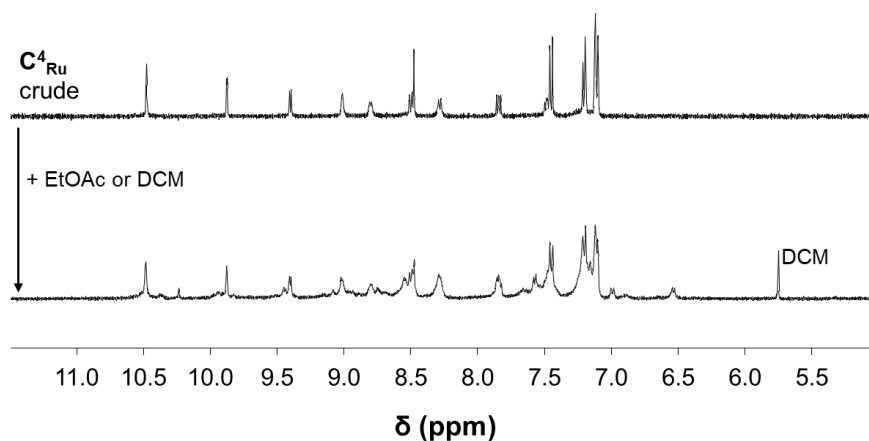


**Figure S33.** Stacked <sup>1</sup>H NMR spectra (400 MHz, DMSO-*d*<sub>6</sub>, 298 K) of the crude reaction mixture of **C<sup>4</sup><sub>Ru</sub>** after 24 h, and of the solid product obtained after addition of EtOAc or DCM. The workup of this compound was done using the same methods as for **C<sup>4</sup><sub>Pt</sub>**.

## Opening and closing reactions

To assess the abilities of MSAs **C<sup>4</sup><sub>Pt</sub>** and **C<sup>4</sup><sub>Ru</sub>** to open and close in the presence of external stimuli, NMR titrations were carried out with 4-(dimethylamino)pyridine (DMAP) to open the cage and *p*-toluenesulfonic acid (*p*-TsOH) to close it. MSA concentrations were 2 mM and DMAP and *p*-TsOH stock concentrations were 100 mM.

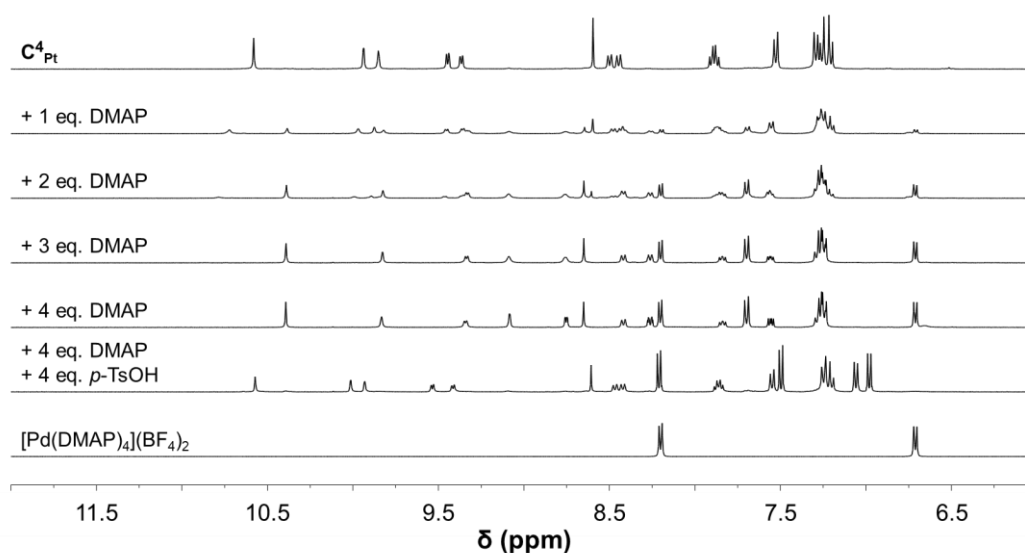


**Figure S34.** Stacked <sup>1</sup>H NMR spectra (400 MHz, DMSO-*d*<sub>6</sub>, 298 K) of the titration of DMAP into a solution of **C<sup>4</sup><sub>Pt</sub>** (2 mM), followed by addition of 4 eq. of *p*-TsOH.

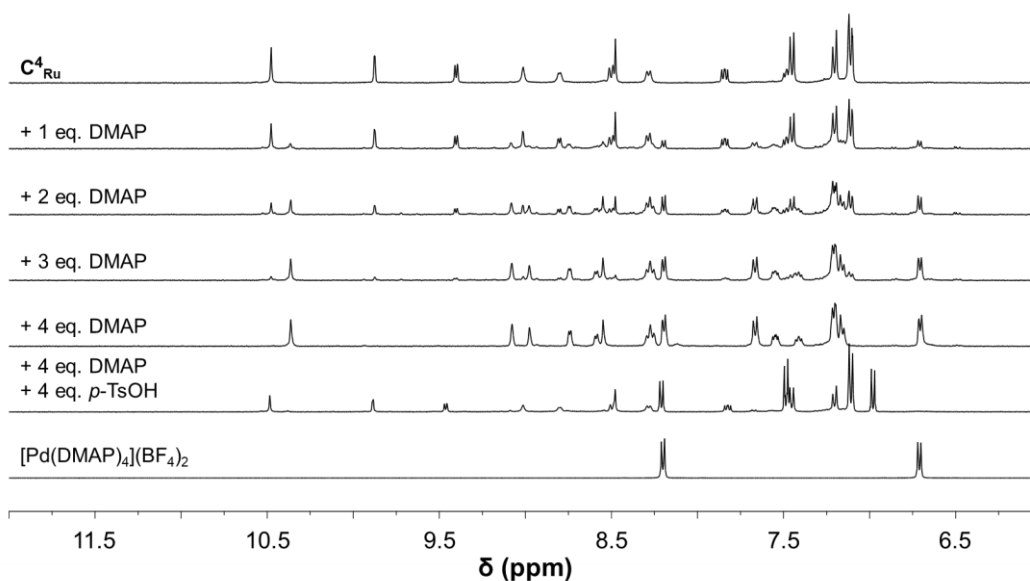


**Figure S35.** Stacked <sup>1</sup>H NMR spectra (400 MHz, DMSO-*d*<sub>6</sub>, 298 K) of the titration of DMAP into a solution of C<sup>4</sup><sub>Ru</sub> (2 mM), followed by addition of 4 eq. of *p*-TsOH.

## Guest binding studies

For C<sup>4</sup><sub>Pt</sub>, stock solutions of 2 mM were prepared in DMSO-*d*<sub>6</sub>, whereas for C<sup>4</sup><sub>Ru</sub> a 3.3 mM stock solution was diluted with DMSO-*d*<sub>6</sub> to 2 mM. Stock solutions of the guests were prepared to concentrations of 100 mM. Each titration step was done by adding 0.2 eq. for sodium mesylate, 0.5 eq. for sodium tosylate, and 0.2 eq. for disodium 1,5-naphthalenedisulfonate. <sup>1</sup>H NMR spectra were recorded immediately after addition of the guest solution and shaking the sample. Guest binding was monitored by tracking the changes in chemical shifts of protons H-1, H-2, H-5, H-11, H-14, and H-15, except for the titration of C<sup>4</sup><sub>Ru</sub> with NDS, in which the shift of proton H-3 was also included. The binding constants were calculated using BindFit v0.5 on <http://supramolecular.org> considering only the shifts of protons in the interior cavities of the cages.<sup>[9]</sup> For MsO and TsO, a 1:2 H:G curve fitting method was used whereas for NDS a 1:1 curve fitting method was used. For binding constant calculations, only the internally facing protons were considered.

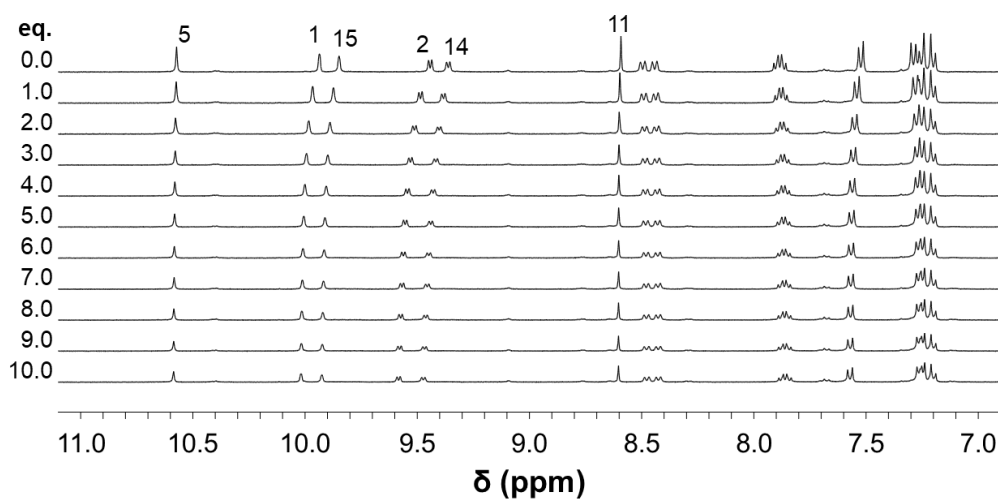


**Figure S36.**  $^1\text{H}$  NMR (400 MHz,  $\text{DMSO-}d_6$ , 298 K) spectra for the titration of MsONa into  $\text{C}^4\text{Pt}$  (2 mM).

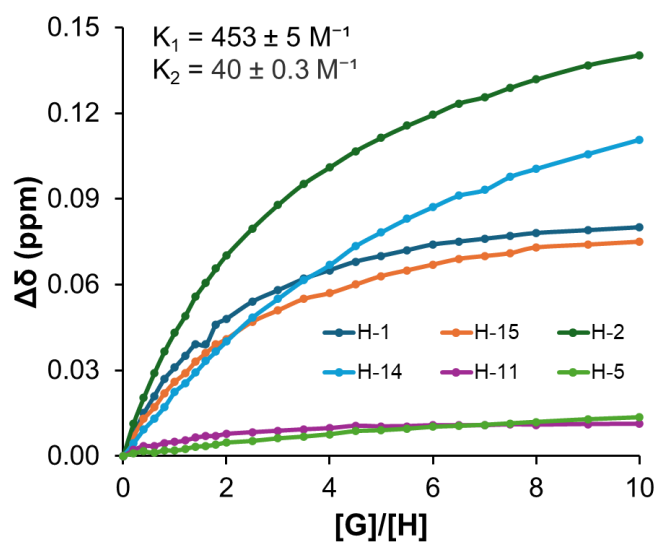


**Figure S37.** Changes in chemical shifts of protons H-1, H-2, H-5, H-11, H-14, and H-15 in the  $^1\text{H}$  NMR (400 MHz,  $\text{DMSO-}d_6$ , 298 K) spectra of  $\text{C}^4\text{Pt}$  (2 mM) during titration with MsONa.

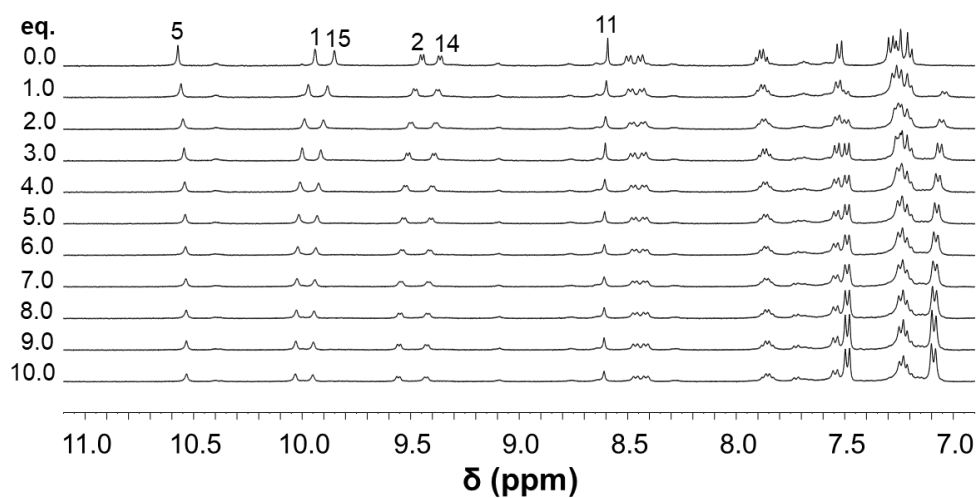


**Figure S38.**  $^1\text{H}$  NMR (400 MHz,  $\text{DMSO-}d_6$ , 298 K) spectra for the titration of TsONa into  $\text{C}^4\text{Pt}$  (2 mM).

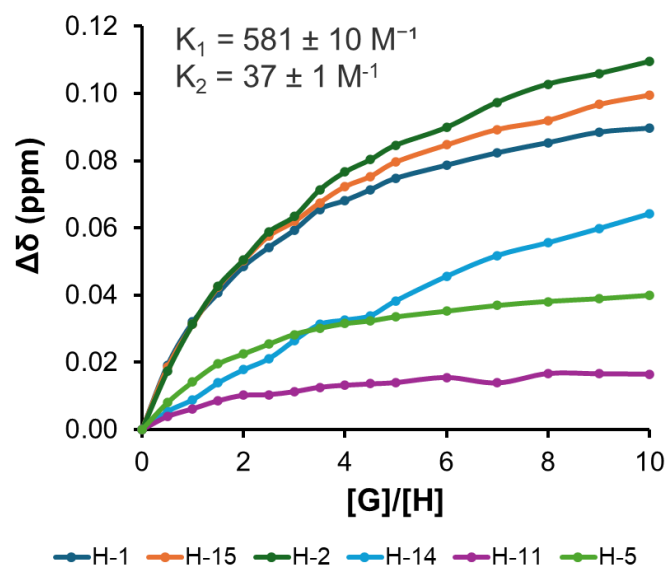


**Figure S39.** Changes in chemical shifts of protons H-1, H-2, H-5, H-11, H-14, and H-15 in the  $^1\text{H}$  NMR (400 MHz,  $\text{DMSO-}d_6$ , 298 K) spectra of  $\text{C}^4\text{Pt}$  (2 mM) during titration with TsONa.

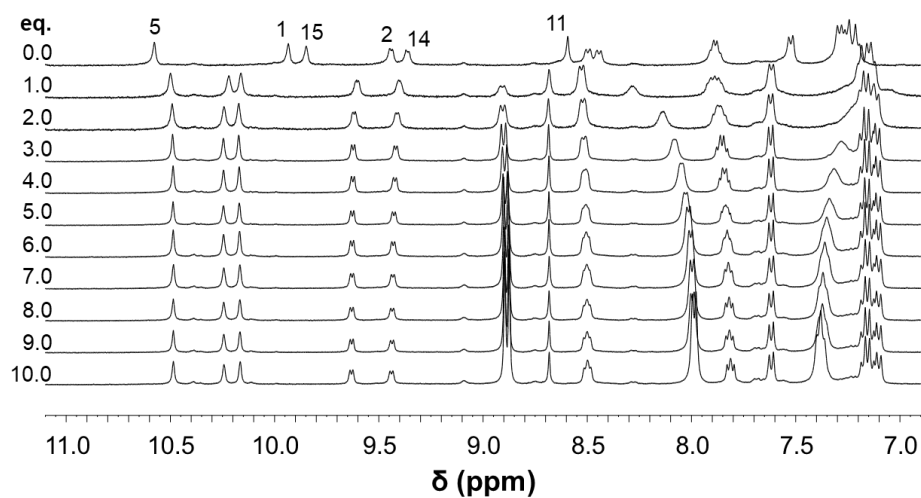


**Figure S40.**  $^1\text{H}$  NMR (400 MHz,  $\text{DMSO-}d_6$ , 298 K) spectra for the titration of **NDS** into **C<sup>4</sup>Pt** (2 mM).

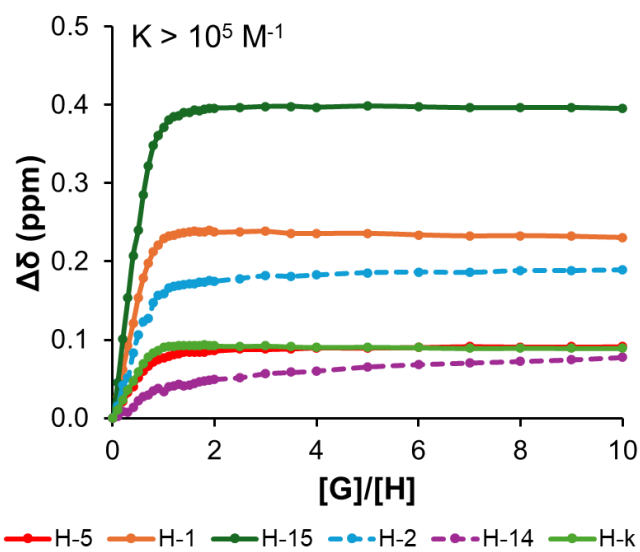


**Figure S41.** Changes in chemical shifts of protons H-1, -2, -5, -11, -14, and -15 in the  $^1\text{H}$  NMR (400 MHz,  $\text{DMSO-}d_6$ , 298 K) spectra of **C<sup>4</sup>Pt** (2 mM) during titration with **NDS**.

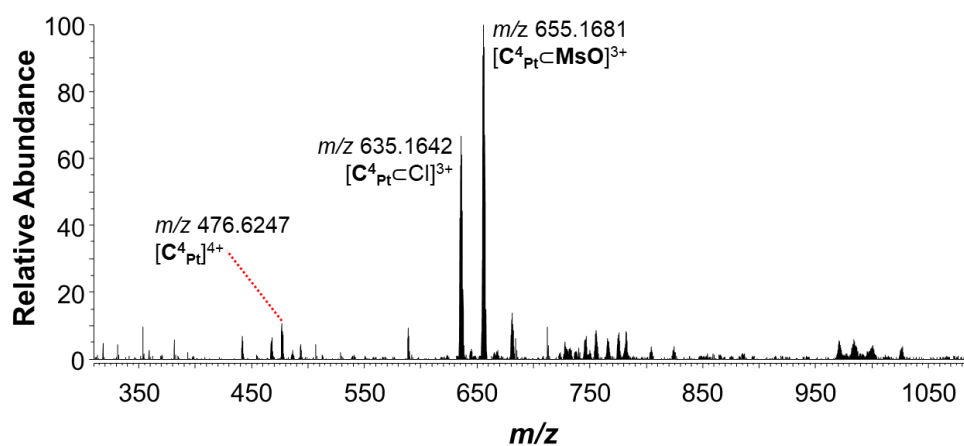


Figure S42. HR-ESI-mass spectrum (DMSO/MeCN) of a 1:1 mixture of  $C^4_{Pt}$  and  $MsO$ .

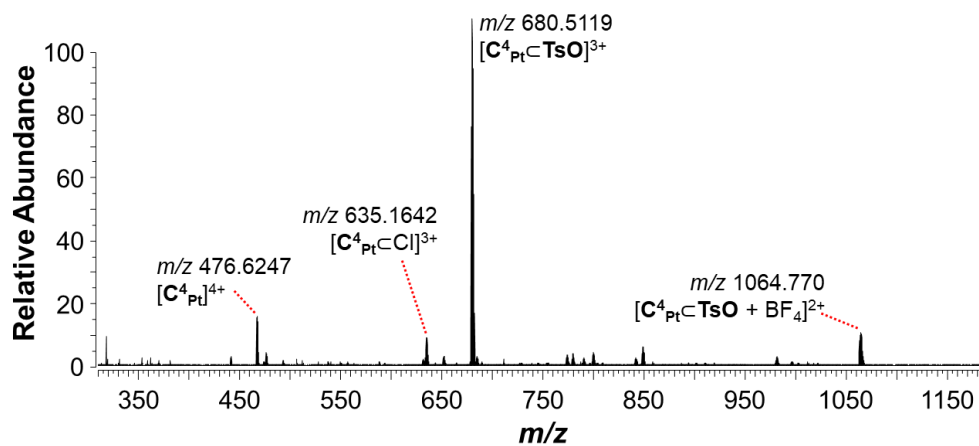


Figure S43. HR-ESI-mass spectrum (DMSO/MeCN) of a 1:1 mixture of  $C^4_{Pt}$  and  $TsO$ .

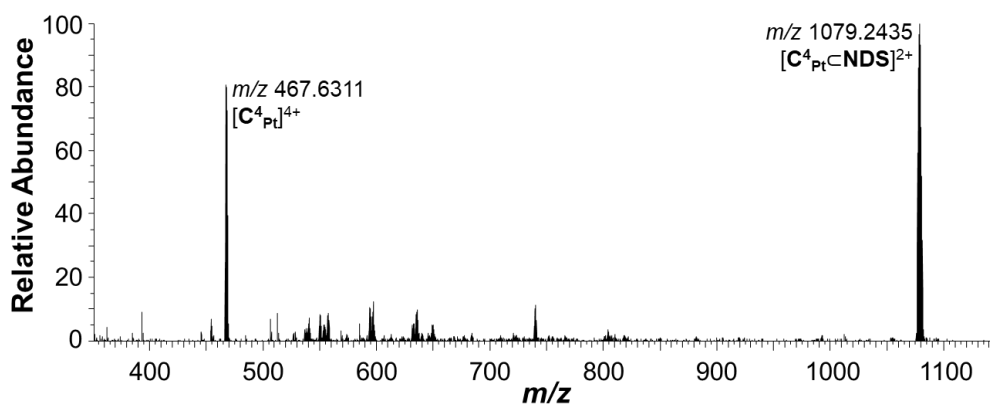
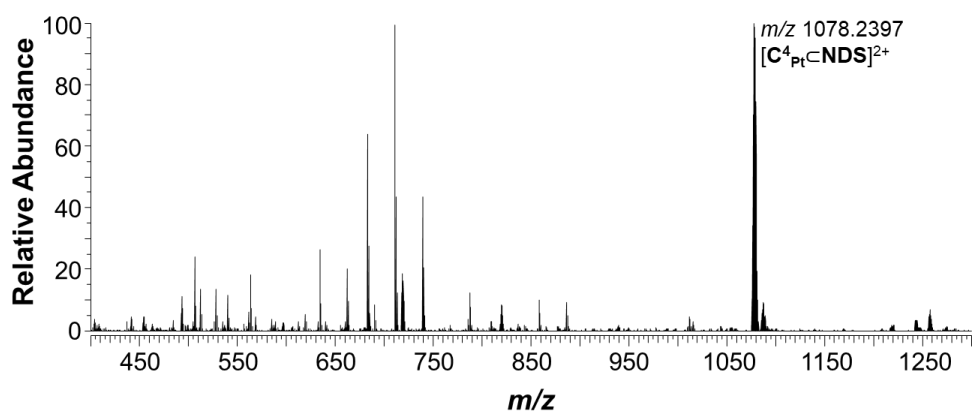
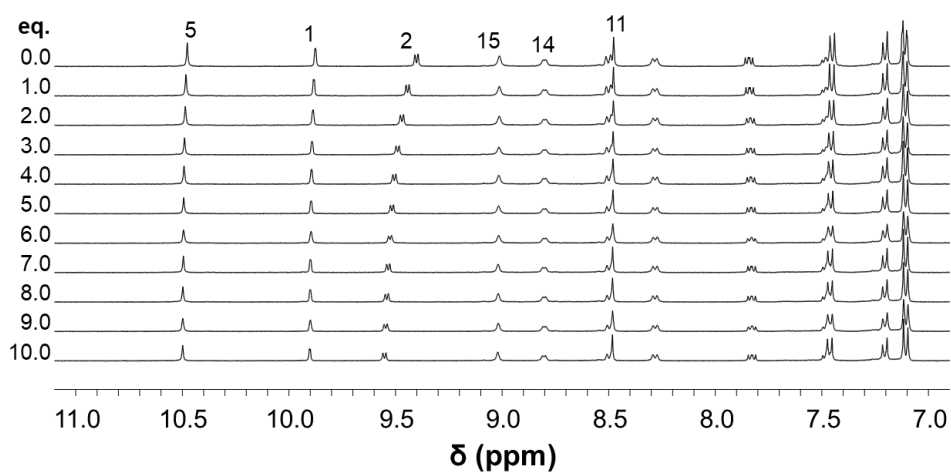


Figure S44. HR-ESI-mass spectrum (DMSO/MeCN) of a 1:1 mixture of  $C^4_{Pt}$  and  $NDS$ .



**Figure S45.** HR-ESI-mass spectrum (DMSO/MeCN) of a 1:1:1:1 mixture of  $C^4_{Pt}$  and **NDS**, **TsO**, and **MsO**.



**Figure S46.**  $^1H$  NMR (400 MHz, DMSO- $d_6$ , 298 K) spectra for the titration of MsONa into  $C^4_{Ru}$  (2 mM).

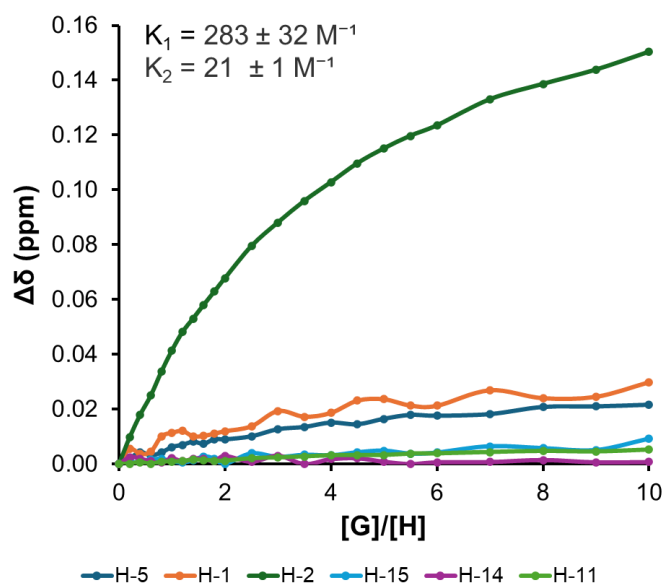


**Figure S47.** Changes in chemical shifts of protons H-1, H-2, H-5, H-11, H-14, and H-15 in the  $^1\text{H}$  NMR (400 MHz,  $\text{DMSO-}d_6$ , 298 K) spectra of  $\text{C}^4\text{Ru}$  (2 mM) during titration with MsONa.

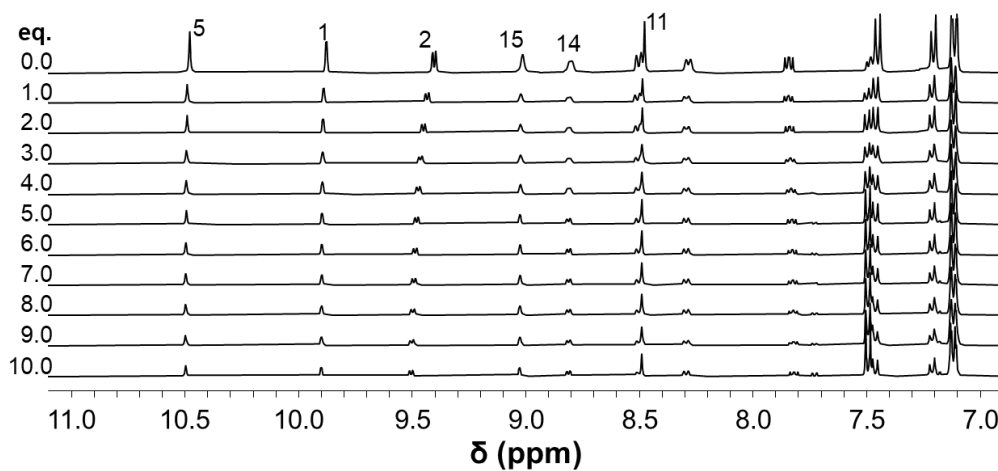


**Figure S48.**  $^1\text{H}$  NMR (400 MHz,  $\text{DMSO-}d_6$ , 298 K) spectra for the titration of TsONa into  $\text{C}^4\text{Ru}$  (2 mM).

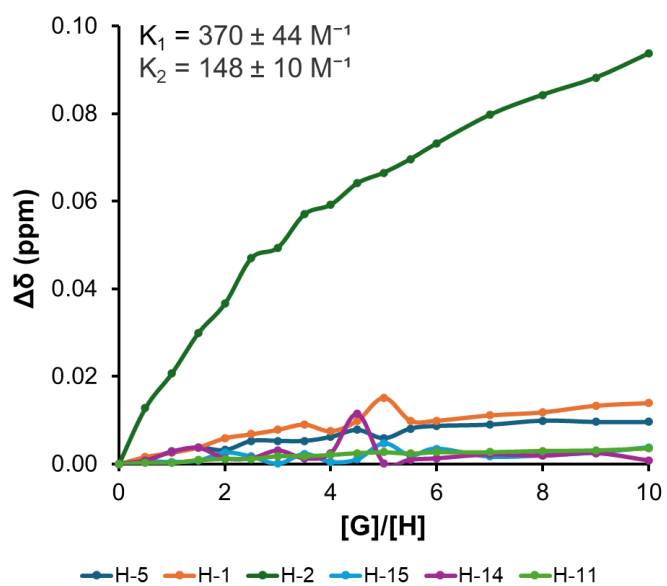


**Figure S49.** Changes in chemical shifts of protons H-1, H-2, H-5, H-11, H-14, and H-15 in the  $^1\text{H}$  NMR (400 MHz,  $\text{DMSO-}d_6$ , 298 K) spectra of  $\text{C}^4\text{Ru}$  (2 mM) during titration with TsONa.

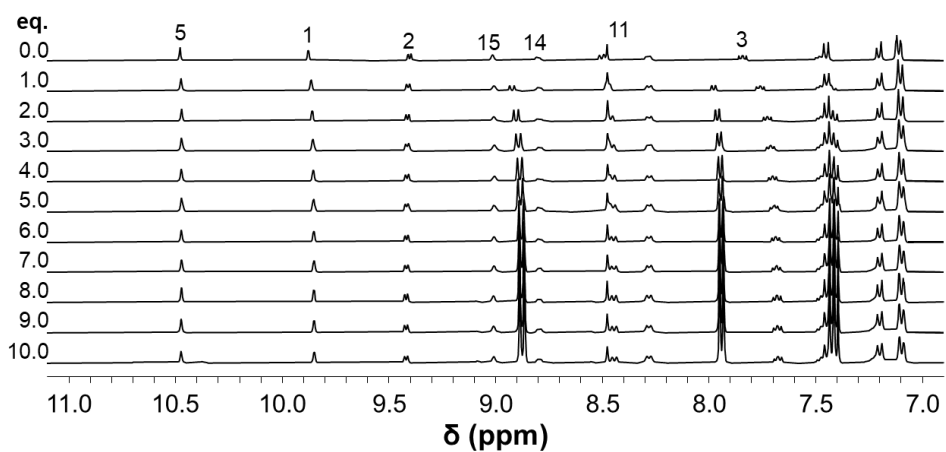


**Figure S50.**  $^1\text{H}$  NMR (400 MHz,  $\text{DMSO-}d_6$ , 298 K) spectra for the titration of NDS into  $\text{C}^4\text{Ru}$  (2 mM).

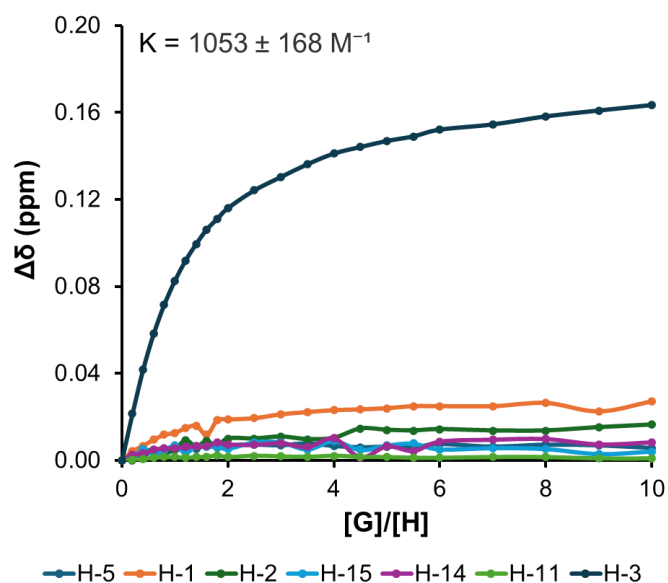


**Figure S51.** Changes in chemical shifts of protons H-1, H-2, H-5, H-11, H-14, H-15, and H-3 in the  $^1\text{H}$  NMR (400 MHz,  $\text{DMSO-}d_6$ , 298 K) spectra of  $\text{C}^4_{\text{Ru}}$  (2 mM) during titration with **NDS**.

## Cisplatin, oxaliplatin and 5-fluorouracil as guests

For cisplatin (**cis**), oxaliplatin (**ox**), and 5-fluorouracil (**5-FU**), mixtures of  $\text{C}^4_{\text{Pt}}$  (approx. 2 mg) and guest (approx. 5 mg) were sonicated in 500  $\mu\text{L}$  of  $\text{CD}_3\text{CN}$  for 30 min after which the suspensions were filtered to obtain host:guest adducts. In the case of  $\text{C}^4_{\text{Ru}}$ , 50  $\mu\text{L}$  of a 16.66 mg/mL solution in DMSO was added to a suspension of cisplatin, oxaliplatin, or 5-fluorouracil in  $\text{CD}_3\text{CN}$  (450  $\mu\text{L}$ ) and the mixtures were sonicated. After 30 min the suspensions were filtered. After sample preparation,  $^1\text{H}$  NMR spectra were collected for all host-guest mixtures.

Mass spectrometric binding studies were conducted at a desolvation temperature of 50  $^\circ\text{C}$  as outlined in the general experimental section. Stock solutions (2.25 mM) of **cis** ( $\text{DMF}/\text{CH}_3\text{CN}$  1:1), **ox** ( $\text{H}_2\text{O}/\text{CH}_3\text{CN}$  1:1) and **5-FU** ( $\text{CH}_3\text{CN}$ ) were prepared. To make stock solutions of the MSAs,  $\text{C}^4_{\text{Pt}}$  and  $\text{C}^4_{\text{Ru}}$  (0.225 mM) were dissolved in 2%  $\text{DMSO}/\text{CH}_3\text{CN}$ . The interactions with the guests were investigated at a ratio of 1:5.

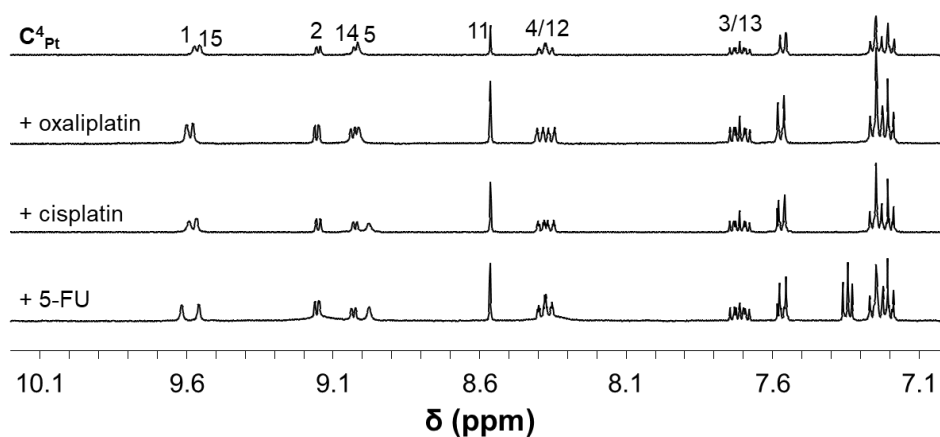


**Figure S52.** Stacked  $^1\text{H}$  NMR spectra (400 MHz,  $\text{CD}_3\text{CN}$ , 298 K) of  $\text{C}^4_{\text{Pt}}$  and mixtures with oxaliplatin, cisplatin and 5-fluorouracil.

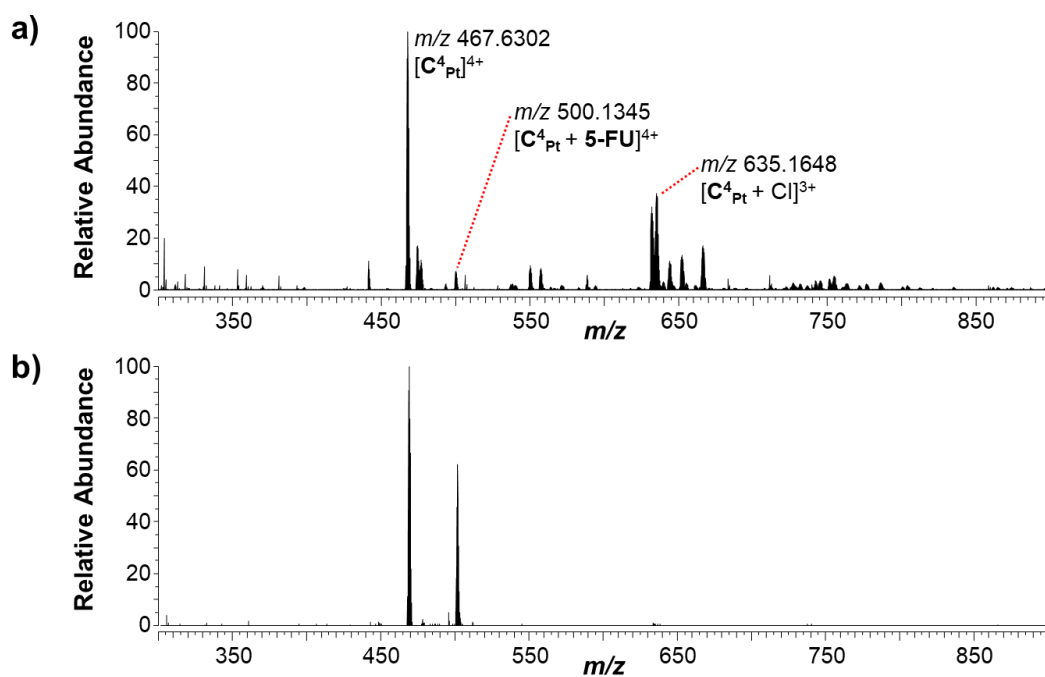


**Figure S53.** a) HR-ESI-mass spectrum (DMSO/ $\text{CH}_3\text{CN}$ ) of a 1:5 mixture of  $\text{C}^4_{\text{Pt}}$  and 5-FU. b) HR-ESI-HCD-mass spectra of the 1:1  $\text{C}^4_{\text{Pt}}:5\text{-FU}$  host-guest adduct at NCE 10.

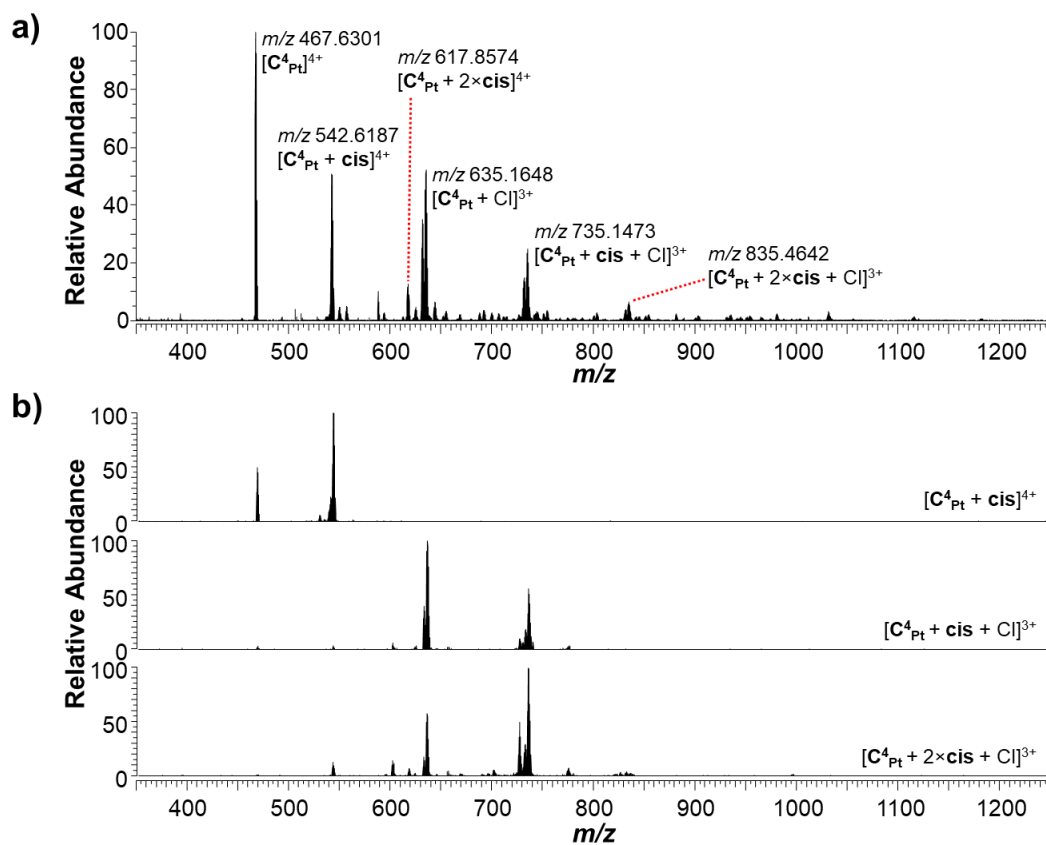


**Figure S54.** a) HR-ESI-mass spectrum (DMSO/CH<sub>3</sub>CN) of a 1:5 mixture of C<sup>4</sup>Pt and cis. b) HR-ESI-HCD-mass spectra of the 1:1, 1:1 + Cl<sup>-</sup>, and 1:2 + Cl<sup>-</sup> C<sup>4</sup>Pt:cis host-guest adducts at NCE 10.

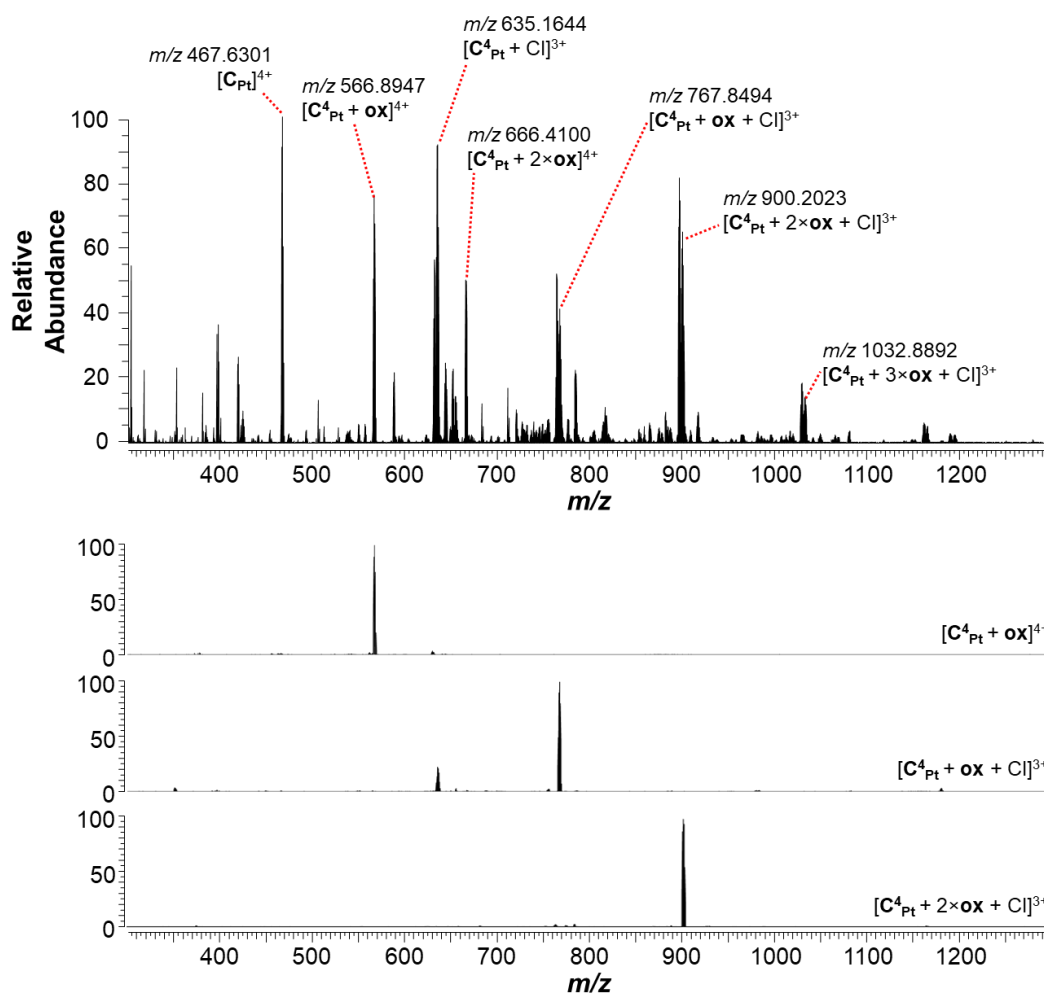


**Figure S55.** a) HR-ESI-mass spectrum (DMSO/CH<sub>3</sub>CN) of a 1:5 mixture of  $\text{C}_{\text{Pt}}^4$  and  $\text{ox}$ . b) HR-ESI-HCD-mass spectra of the 1:1, 1:1 + Cl<sup>-</sup>, and 1:2 + Cl<sup>-</sup>  $\text{C}_{\text{Pt}}:\text{ox}$  host-guest adducts at NCE 10.

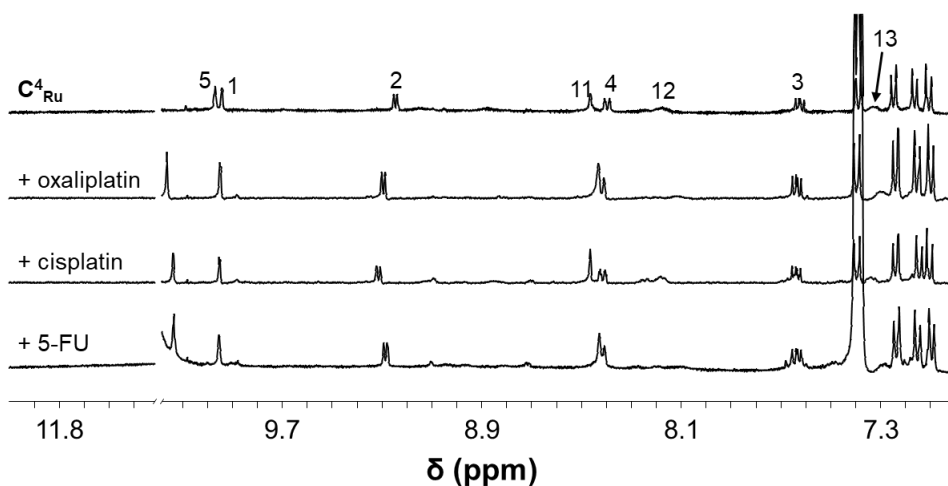


**Figure S56.** Stacked  $^1\text{H}$  NMR spectra (400 MHz,  $\text{CD}_3\text{CN}$ , 298 K) of  $\text{C}^4_{\text{Ru}}$  and mixtures with oxaliplatin, cisplatin and 5-fluorouracil. High-intensity peaks of 5-FU have been cut from the spectrum for clarity. Intense broadening of protons H-14 and H-15 (those pointing towards the *endo* and *exo* chlorido ligands) was observed.

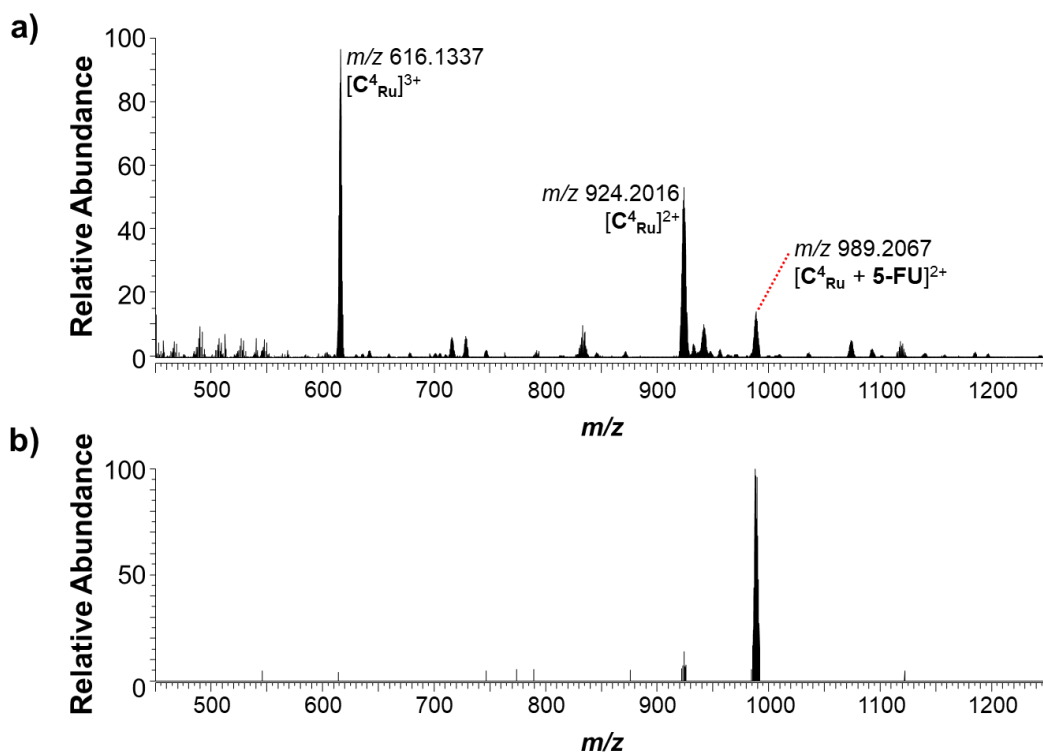


**Figure S57.** a) HR-ESI-mass spectrum (DMSO/ $\text{CH}_3\text{CN}$ ) of a 1:5 mixture of  $\text{C}^4_{\text{Ru}}$  and **5-FU**. b) HR-ESI-HCD-mass spectra of the 1:1,  $\text{C}^4_{\text{Ru}}$ :**5-FU** host-guest adduct at NCE 10.

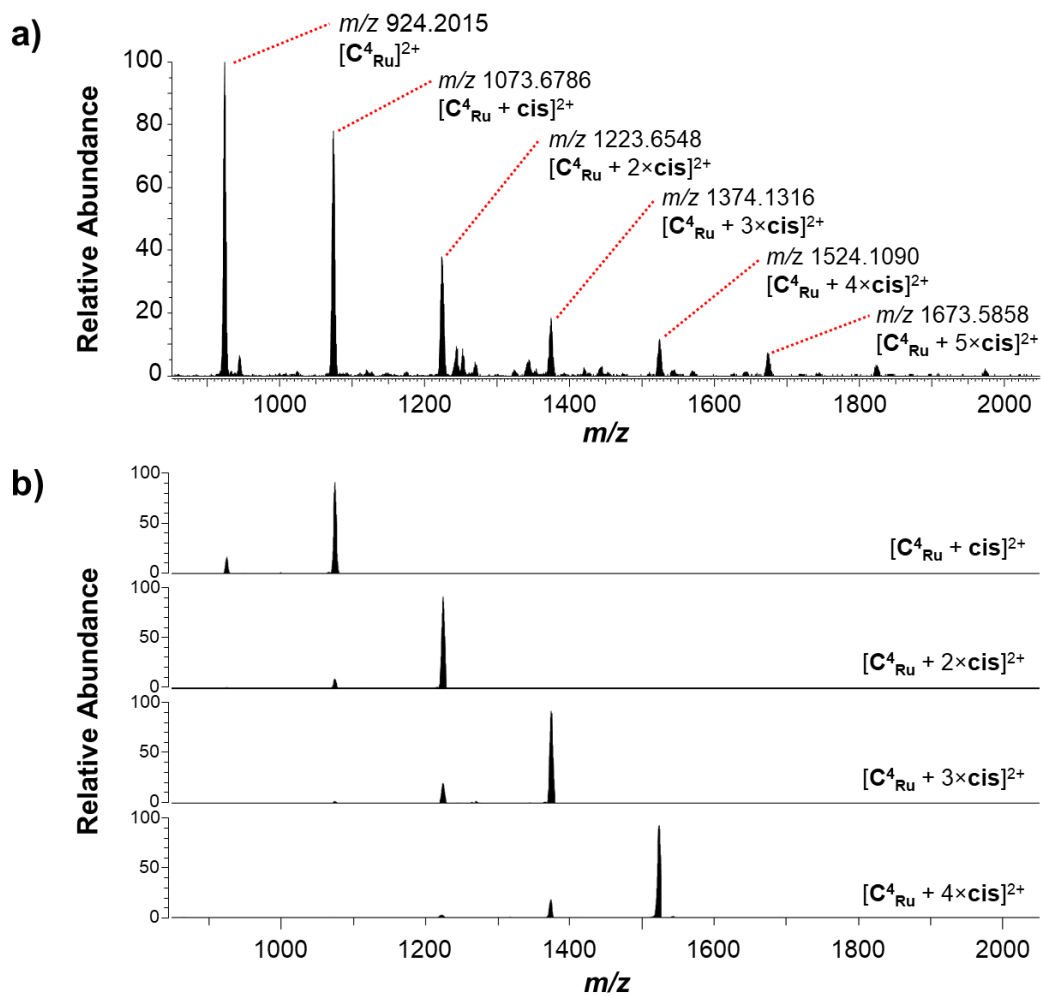


**Figure S58.** a) HR-ESI-mass spectrum (DMSO/CH<sub>3</sub>CN) of a 1:5 mixture of C<sup>4</sup><sub>Ru</sub> and cis. b) HR-ESI-HCD-mass spectra of 1:1, 1:2, 1:3, and 1:4 C<sup>4</sup><sub>Ru</sub>:cis host-guest adducts at NCE 10.

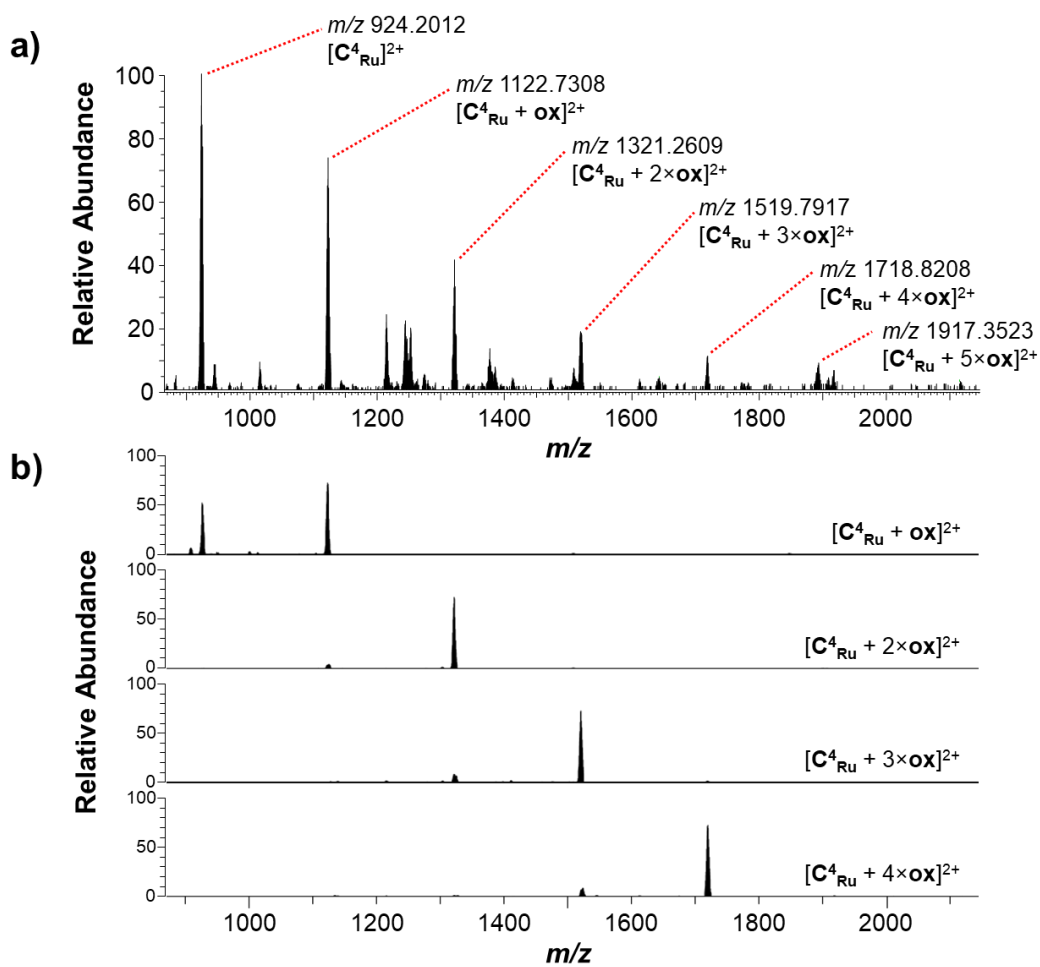


**Figure S59.** HR-ESI-mass spectrum (DMSO/CH<sub>3</sub>CN) of a 1:5 mixture of C<sub>4</sub>Ru and ox. b) HR-ESI-HCD-mass spectra of 1:1, 1:2, 1:3, and 1:4 C<sub>4</sub>Ru:ox host-guest adducts at NCE 10.

**Table S1.** Host-guest species detected for the reactions between  $C^4_{Pt}$  and  $C^4_{Ru}$  with **MsO**, **TsO**, **NDS**, **cis**, **ox** and **5-FU** by ESI-MS.

<b>Species</b>	<b><i>m/z</i><sub>obs</sub></b>	<b><i>m/z</i><sub>calc</sub></b>	<b>Error (ppm)</b>
$[C^4_{Pt} - 4BF_4]^{4+}$	467.6310	467.6311	0.2
$[C^4_{Pt} - 4BF_4 + Cl]^{3+}$	635.1648	635.1646	0.3
$[C^4_{Pt} - 4BF_4 + MsO]^{3+}$	655.1681	655.1684	0.5
$[C^4_{Pt} - 4BF_4 + TsO]^{3+}$	680.5120	680.5121	0.1
$[C^4_{Pt} - 4BF_4 + NDS]^{3+}$	1079.2427	1079.2432	0.5
$[C^4_{Pt} - 4BF_4 + 5-FU]^{4+}$	500.1345	500.1355	2.0
$[C^4_{Pt} - 4BF_4 + cis]^{4+}$	542.6187	542.6195	1.5
$[C^4_{Pt} - 4BF_4 + 2 \times cis]^{4+}$	617.8574	617.8580	1.0
$[C^4_{Pt} - 4BF_4 + cis + Cl]^{3+}$	735.1473	735.1492	2.6
$[C^4_{Pt} - 4BF_4 + ox]^{4+}$	566.8947	566.8960	2.3
$[C^4_{Pt} - 4BF_4 + 2 \times ox]^{4+}$	666.4100	666.4111	1.7
$[C^4_{Pt} - 4BF_4 + ox + Cl]^{3+}$	767.8494	767.8510	2.1
$[C^4_{Pt} - 4BF_4 + 2 \times ox + Cl]^{3+}$	900.2023	900.2042	2.1
$[C^4_{Pt} - 4BF_4 + 3 \times ox + Cl]^{3+}$	1032.8892	1032.8911	1.8
$[C^4_{Ru} - 2BF_4]^{2+}$	924.2009	924.2011	0.2
$[C^4_{Ru} - 2BF_4 + 5-FU]^{2+}$	989.2067	989.2101	2.9
$[C^4_{Ru} - 2BF_4 + cis]^{2+}$	1073.6786	1073.6783	0.3
$[C^4_{Ru} - 2BF_4 + 2 \times cis]^{2+}$	1223.6548	1223.6551	0.3
$[C^4_{Ru} - 2BF_4 + 3 \times cis]^{2+}$	1374.1316	1374.1319	0.2
$[C^4_{Ru} - 2BF_4 + 4 \times cis]^{2+}$	1524.1090	1524.1087	0.2
$[C^4_{Ru} - 2BF_4 + 5 \times cis]^{2+}$	1673.5858	1673.5856	0.1
$[C^4_{Ru} - 2BF_4 + 6 \times cis]^{2+}$	1824.0624	1824.0623	0.1
$[C^4_{Ru} - 2BF_4 + ox]^{2+}$	1122.7308	1122.7313	0.4
$[C^4_{Ru} - 2BF_4 + 2 \times ox]^{2+}$	1321.2609	1321.2612	0.2
$[C^4_{Ru} - 2BF_4 + 3 \times ox]^{2+}$	1519.7917	1519.7911	0.4
$[C^4_{Ru} - 2BF_4 + 4 \times ox]^{2+}$	1718.8208	1718.8213	0.3
$[C^4_{Ru} - 2BF_4 + 5 \times ox]^{2+}$	1917.3523	1917.3512	0.5

## X-ray crystallographic data

**Table S2.** Crystal and measurement parameters for **C<sup>4</sup>Pt**, **C<sup>4</sup>Pt<sub>Cl</sub>NDS** and **C<sup>4</sup>Ru**.

Parameter	C <sup>4</sup> Pt	C <sup>4</sup> Pt <sub>Cl</sub> NDS	C <sup>4</sup> Ru
CCDC number	2389021	2389022	2389023
Empirical formula	C <sub>100</sub> H <sub>80</sub> N <sub>16</sub> O <sub>4</sub> PdPtB <sub>4</sub> F <sub>16</sub> [+4 DMF]	C <sub>100</sub> H <sub>80</sub> B <sub>2</sub> F <sub>8</sub> N <sub>16</sub> O <sub>4</sub> PdPt·C <sub>10</sub> H <sub>6</sub> O <sub>6</sub> S <sub>2</sub> · C <sub>3</sub> H <sub>7</sub> NO [+5 DMF]	C <sub>100</sub> H <sub>80</sub> Cl <sub>2</sub> N <sub>16</sub> O <sub>4</sub> PdRu· C <sub>2</sub> H <sub>6</sub> OS [+8 DMSO]
Formula weight / g/mol	2514.94	2769.75	2551.31
Temperature / K	100.0(6)	119.99(13)	100.00(10)
Crystal system	monoclinic	triclinic	tetragonal
Space group	<i>P2<sub>1</sub>/m</i>	<i>P</i> -1	<i>P4/ncc</i>
a / Å	9.68300(10)	15.47952(19)	18.0390(3)
b / Å	23.8429(2)	19.9749(3)	18.0390(3)
c / Å	28.0717(4)	21.2142(3)	41.9278(11)
α / °	90	79.4685(11)	90
β / °	99.3850(10)	84.6071(10)	90
γ / °	90	73.5233(11)	90
Volume / Å <sup>3</sup>	6394.19(13)	6177.96(14)	13643.5(6)
Z	2	2	4
ρ <sub>calc</sub> / g/cm <sup>3</sup>	1.306	1.489	1.242
μ / mm <sup>-1</sup>	3.840	4.301	4.085
F(000)	2552.0	2832.0	5304.0

**Table S2.** Cont'd.

Crystal size / mm <sup>3</sup>	0.18 × 0.10 × 0.08	0.20 × 0.08 × 0.05	0.04 × 0.03 × 0.03
Radiation	Cu Kα (λ = 1.54184)	CuKα (λ = 1.54184)	Cu Kα (λ = 1.54184)
2θ range for data collection / °	7.382 to 136.478	7.47 to 135.478	8.114 to 135.38
Index ranges	-11 ≤ h ≤ 11	-18 ≤ h ≤ 18	-21 ≤ h ≤ 21
	-28 ≤ k ≤ 27	-23 ≤ k ≤ 23	-21 ≤ k ≤ 12
	-33 ≤ l ≤ 33	-25 ≤ l ≤ 25	-50 ≤ l ≤ 46
Reflections collected	84211	191459	46648
Independent reflections	11986 [R <sub>int</sub> = 0.0644, R <sub>sigma</sub> = 0.0375]	22345 [R <sub>int</sub> = 0.0750, R <sub>sigma</sub> = 0.0323]	6182 [R <sub>int</sub> = 0.1033, R <sub>sigma</sub> = 0.0513]
Data/restraints/parameters	11986/346/590	22345/77/1390	6182/98/303
Goodness-of-fit on F <sup>2</sup>	1.122	1.018	0.980
Final R indexes [I ≥ 2σ (I)]	R <sub>1</sub> = 0.0525, wR <sub>2</sub> = 0.1293	R <sub>1</sub> = 0.0512, wR <sub>2</sub> = 0.1339	R <sub>1</sub> = 0.0591, wR <sub>2</sub> = 0.1804
Final R indexes [all data]	R <sub>1</sub> = 0.0616, wR <sub>2</sub> = 0.1338	R <sub>1</sub> = 0.0557, wR <sub>2</sub> = 0.1371	R <sub>1</sub> = 0.0903, wR <sub>2</sub> = 0.2050
Largest diff. peak/hole / e Å <sup>-3</sup>	0.89/-0.77	3.09/-1.16	0.55/-0.40

Single crystals of **C<sup>4</sup><sub>Pt</sub>** and **C<sup>4</sup><sub>Pt</sub>·NDS** were grown by vapor diffusion of toluene into a concentrated solution of **C<sup>4</sup><sub>Pt</sub>** or of **C<sup>4</sup><sub>Pt</sub>** and **NDS** (1:1) in *N,N*-dimethylformamide (DMF; Figures 2 and 5). Crystals of **C<sup>4</sup><sub>Ru</sub>** were obtained by vapor diffusion of EtOAc into 400 μL of a 3.3 mM solution of **C<sup>4</sup><sub>Ru</sub>**.

**Table S3.** Selected average bond lengths observed for MSAs  $C^4_{Pt}$  and  $C^4_{Ru}$  and  $C^4_{Pt} \subset NDS$ .

Bond / Distance	Bond length / Å		
	$C^4_{Pt}$	$C^4_{Ru}$	$C^4_{Pt} \subset NDS$
Ru–Cl	–	2.411(3)	–
Ru–N	–	2.079(4)	–
M–N	2.013(12)	2.028(3)	2.0154(9)
Ru/Pt...Pd	15.484(1)	15.205(1)	15.3792(6)

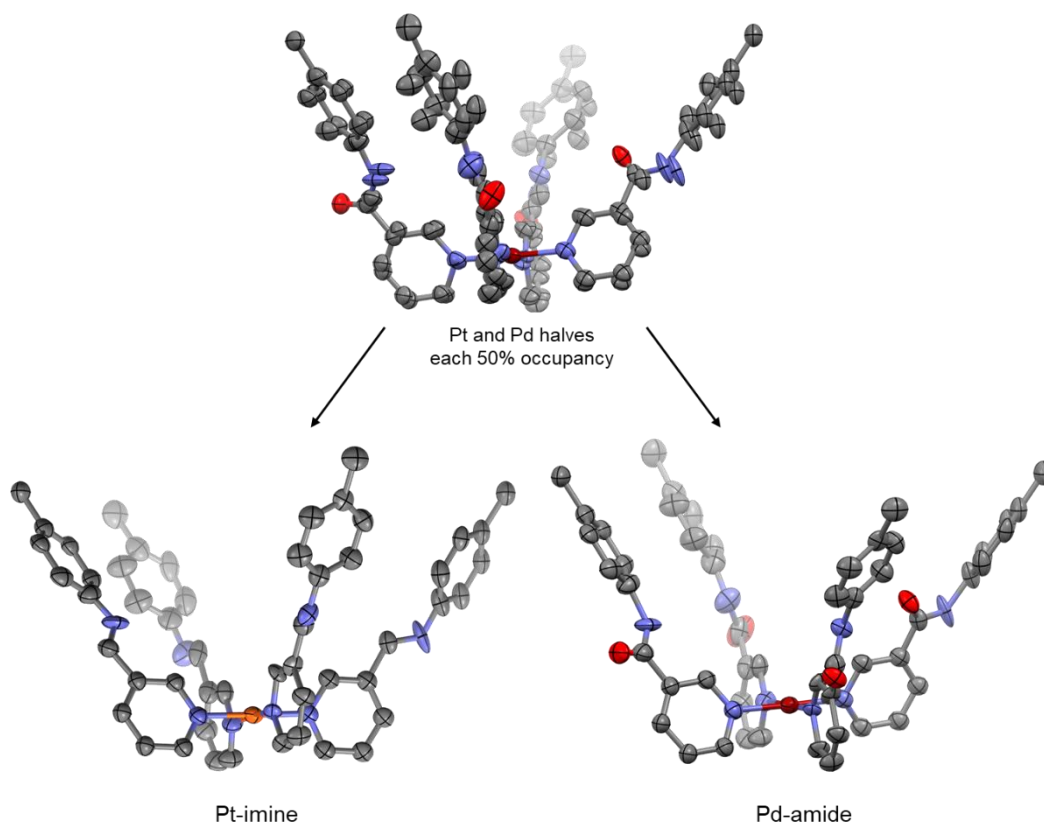


**Figure S60.** Ellipsoid representation of the asymmetric unit of the molecular structure of  $C^4_{Pt}$  where both Pd- and Pt-halves of the cage sit on top of each other, each with occupancies of 50%. Hydrogen atoms and  $BF_4$  counteranions have been omitted for clarity. Ellipsoids are drawn at a 50% probability level.

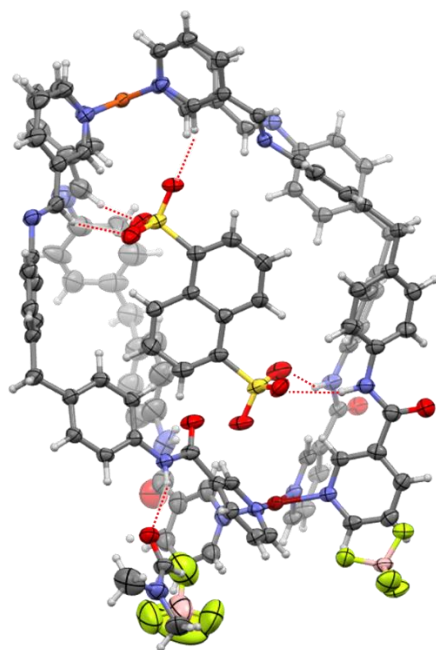


**Figure S61.** Ellipsoid representation of the molecular structure of  $C^4_{Pt}CNDS$ . Hydrogen bonding interactions have been shown as dashed red lines.

## Host-guest MMFF models

All Merck Molecular Force Field (MMFF) models were generated using SPARTAN '24<sup>®</sup>. Cages  $C^4_{Ru}$  and  $C^4_{Pt}$  were modelled with **MsO**, **TsO**, **NDS**, **5-FU**, **cis**, and **ox**.

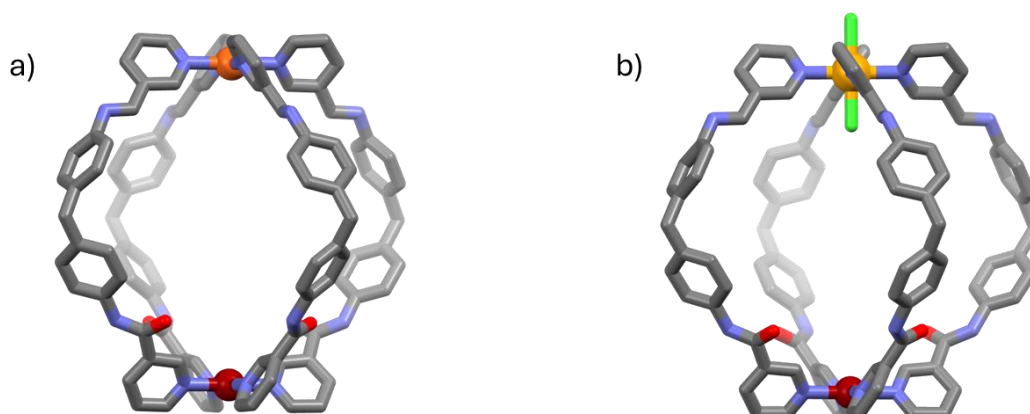


**Figure S62.** SPARTAN '24<sup>®</sup> MMFF models of a)  $C^4_{Pt}$ , and b)  $C^4_{Ru}$ .

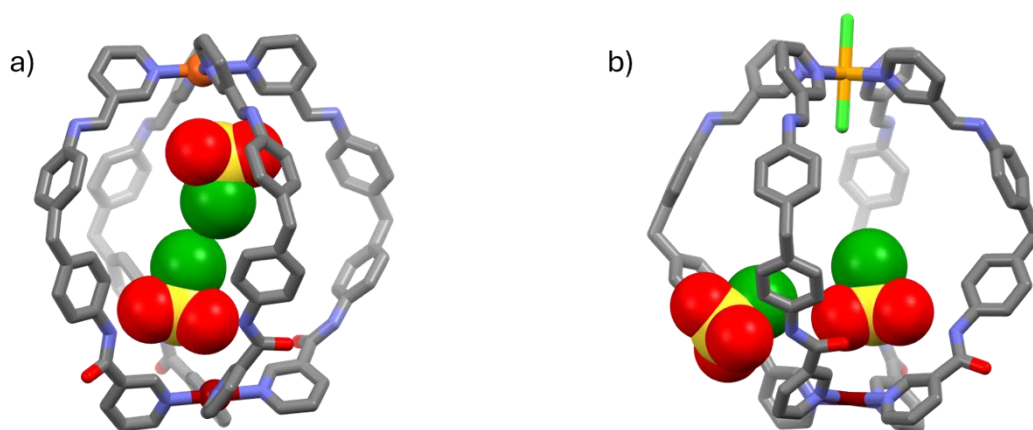


**Figure S63.** SPARTAN '24<sup>®</sup> MMFF models of a)  $C^4_{Pt}C^2MsO$ , and b)  $C^4_{Ru}C^2MsO$ .

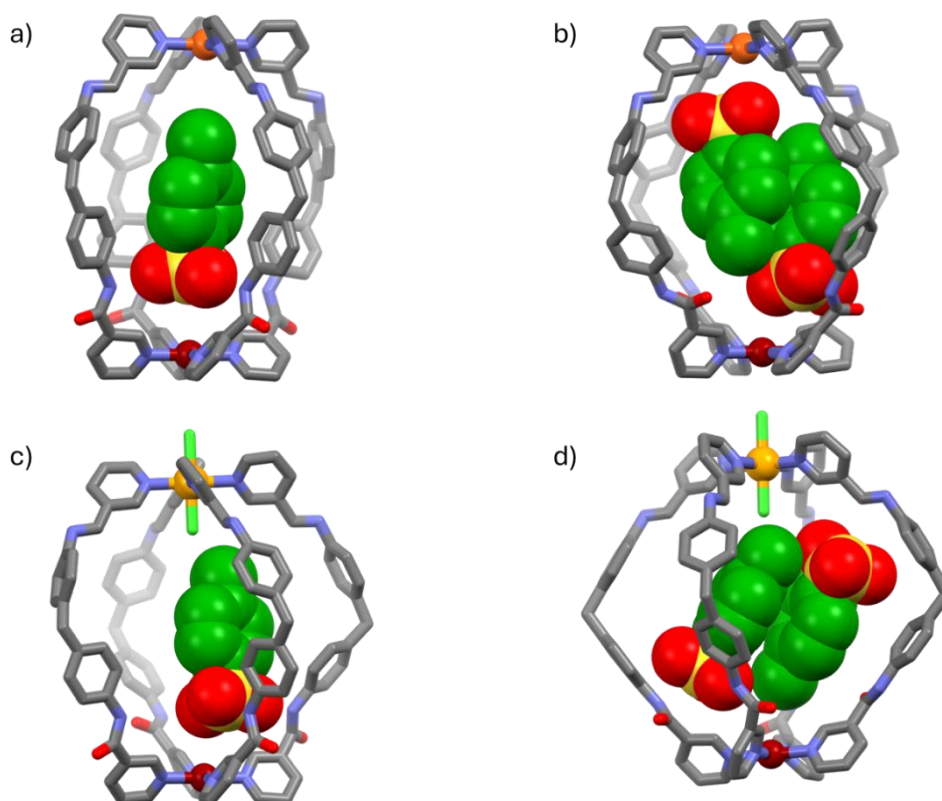


**Figure S64.** SPARTAN '24<sup>®</sup> MMFF models of a)  $C^4_{Pt}C^2TsO$ , b)  $C^4_{Pt}C^2TsO$ , c)  $C^4_{Ru}C^2TsO$ , and d)  $C^4_{Ru}C^2TsO$ .

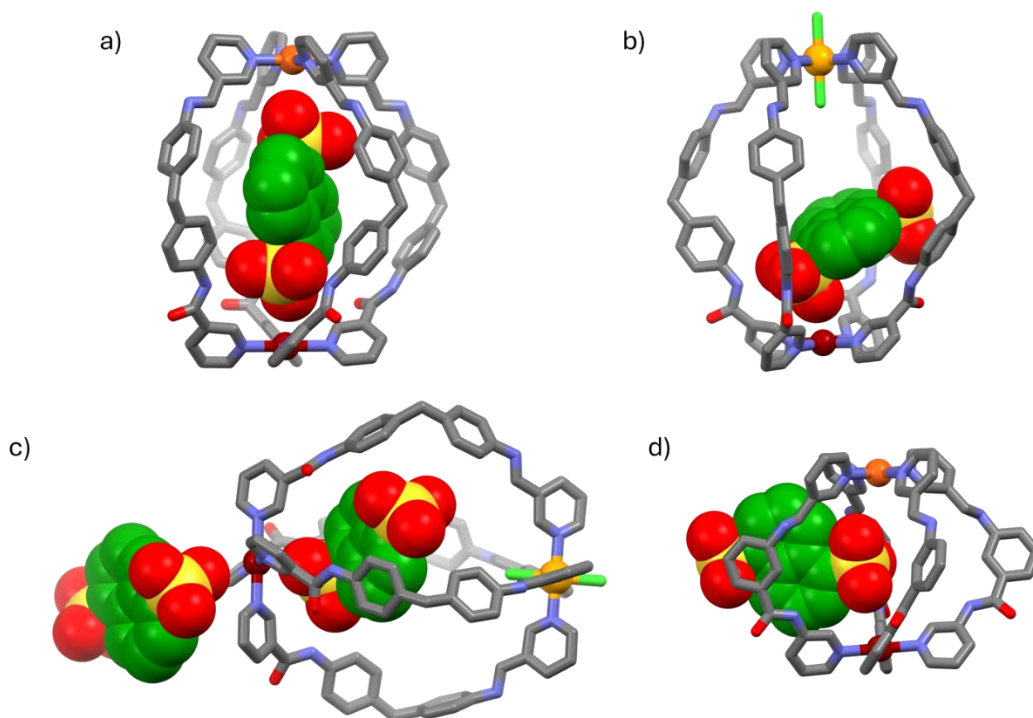


**Figure S65.** SPARTAN '24<sup>®</sup> MMFF models of a)  $C^4_{Pt}CND5$ , b)  $C^4_{Ru}CND5$ , c)  $C^4_{Ru}C2NDS$  and d)  $C^3_{Pt}CND5$ .

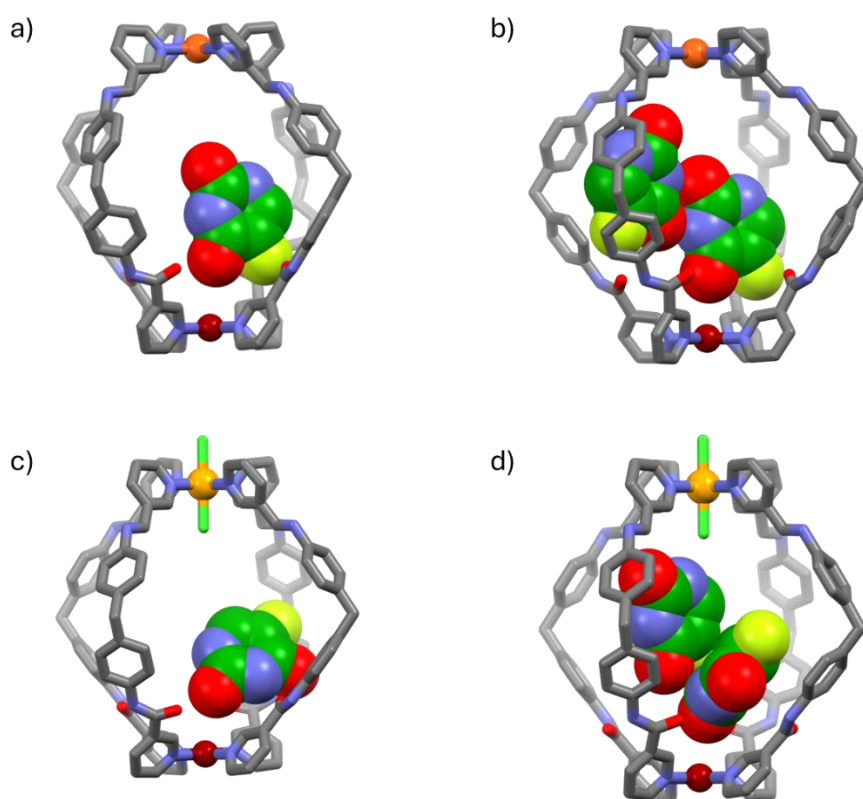


**Figure S66.** SPARTAN '24<sup>®</sup> MMFF models of a)  $C^4_{Pt}C5-FU$ , b)  $C^4_{Pt}C25-FU$ , c)  $C^4_{Ru}C5-FU$ , and d)  $C^4_{Ru}C25-FU$ .

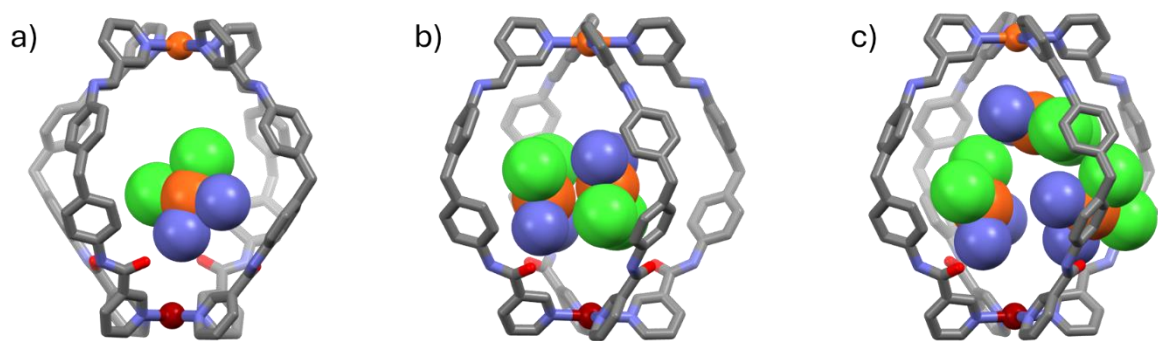


**Figure S67.** SPARTAN '24<sup>®</sup> MMFF models of a)  $C^4_{Pt}C_{cis}$ , b)  $C^4_{Pt}C_{2cis}$ , and c)  $C^4_{Pt}C_{3cis}$ .

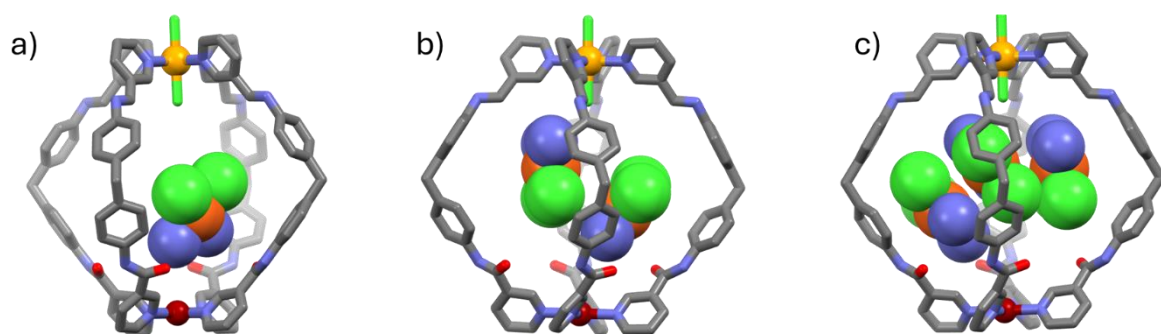


**Figure S68.** SPARTAN '24<sup>®</sup> MMFF models of a)  $C^4_{Ru}C_{cis}$ , b)  $C^4_{Ru}C_{2cis}$ , and c)  $C^4_{Ru}C_{3cis}$ .

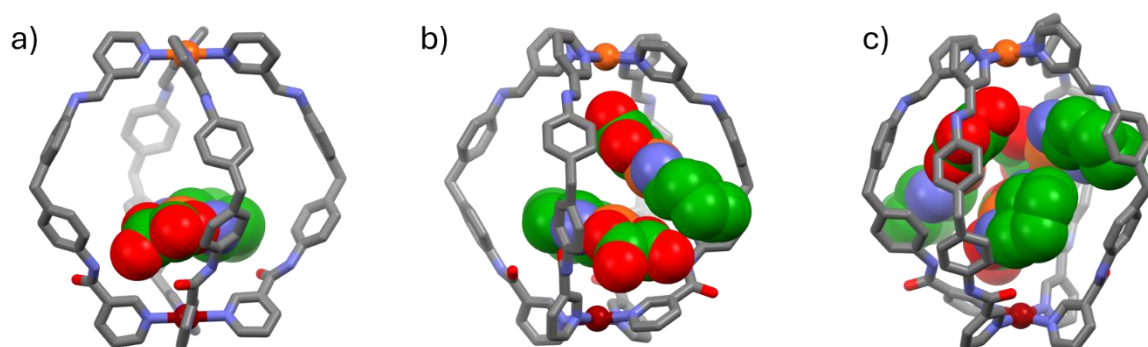


**Figure S69.** SPARTAN '24<sup>®</sup> MMFF models of a)  $C^4_{Pt}CO_x$ , b)  $C^4_{Pt}C_{2O_x}$ , and c)  $C^4_{Pt}C_{3O_x}$ .

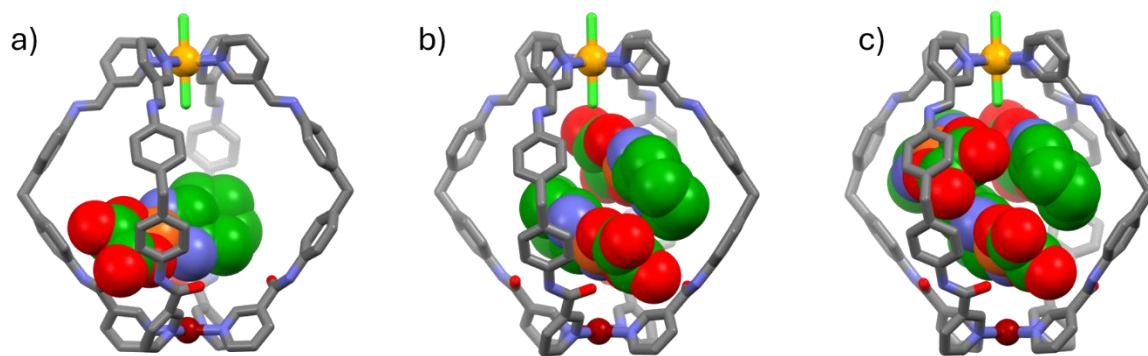


**Figure S70.** SPARTAN '24© MMFF models of a)  $C^4_{Ru}C0x$ , b)  $C^4_{Ru}C20x$ , and c)  $C^4_{Ru}C30x$ .

## References

- [1] J. E. M. Lewis, E. L. Gavey, S. A. Cameron, J. D. Crowley, *Chem. Sci.* **2012**, *3*, 778-784.
- [2] L. S. Lisboa, J. A. Findlay, L. J. Wright, C. G. Hartinger, J. D. Crowley, *Angew. Chem., Int. Ed.* **2020**, *59*, 11101-11107.
- [3] H. B. Gearing, T. Söhnle, P. Young, L. Lisboa, L. J. Wright, J. D. Crowley, C. G. Hartinger, *Chem. Commun.* **2024**, *60*, 10950-10953.
- [4] P. S. Nagle, F. Rodriguez, A. Kahvedžić, S. J. Quinn, I. Rozas, *J. Med. Chem.* **2009**, *52*, 7113-7121.
- [5] S. S. Mishra, S. V. K. Kompella, S. Krishnaswamy, S. Balasubramanian, D. K. Chand, *Inorg. Chem.* **2020**, *59*, 12884-12894.
- [6] G. Sheldrick, *Acta Crystallogr., Sect. A: Found. Adv.* **2015**, *71*, 3-8.
- [7] a) L. J. Bourhis, O. V. Dolomanov, R. J. Gildea, J. A. K. Howard, H. Puschmann, *Acta Crystallogr., Sect. A: Found. Crystallogr.* **2015**, *71*, 59-75; b) O. V. Dolomanov, L. J. Bourhis, R. J. Gildea, J. A. K. Howard, H. Puschmann, *J. Appl. Crystallogr.* **2009**, *42*, 339-341.
- [8] C. F. Macrae, I. Sovago, S. J. Cottrell, P. T. A. Galek, P. McCabe, E. Pidcock, M. Platings, G. P. Shields, J. S. Stevens, M. Towler, P. A. Wood, *J. Appl. Crystallogr.* **2020**, *53*, 226-235.
- [9] a) Supramolecular.Org, <http://supramolecular.org>, ; b) P. Thordarson, *Chem. Soc. Rev.* **2011**, *40*, 1305-1323.